NASA CONTRACT REPORT 159235

NASA-CR-159235

1980 00 11748

WAKE FLOWFIELDS FOR JOVIAN PROBE

CARL D. ENGEL

AND

LEROY M. HAIR

REMTECH INC.

HUNTSVILLE, ALABAMA   35805

CONTRACT NAS1-15819

MARCH 1980

NASA

National Aeronautics and
Space Administration

Langley Research Center
Hampton, Virginia 23665

FOREWORD

This final report presents work which was conducted for Langley Research Center (LaRC) in response to requirements of Contract NAS1-15819. The work presented was performed at REMTECH's Huntsville office and is entitled "Wake Flowfields for Jovian Probe."

The NASA technical coordination for this study was provided by Dr. James Moss of the Aerothermodynamics Branch of the Space Systems Division.
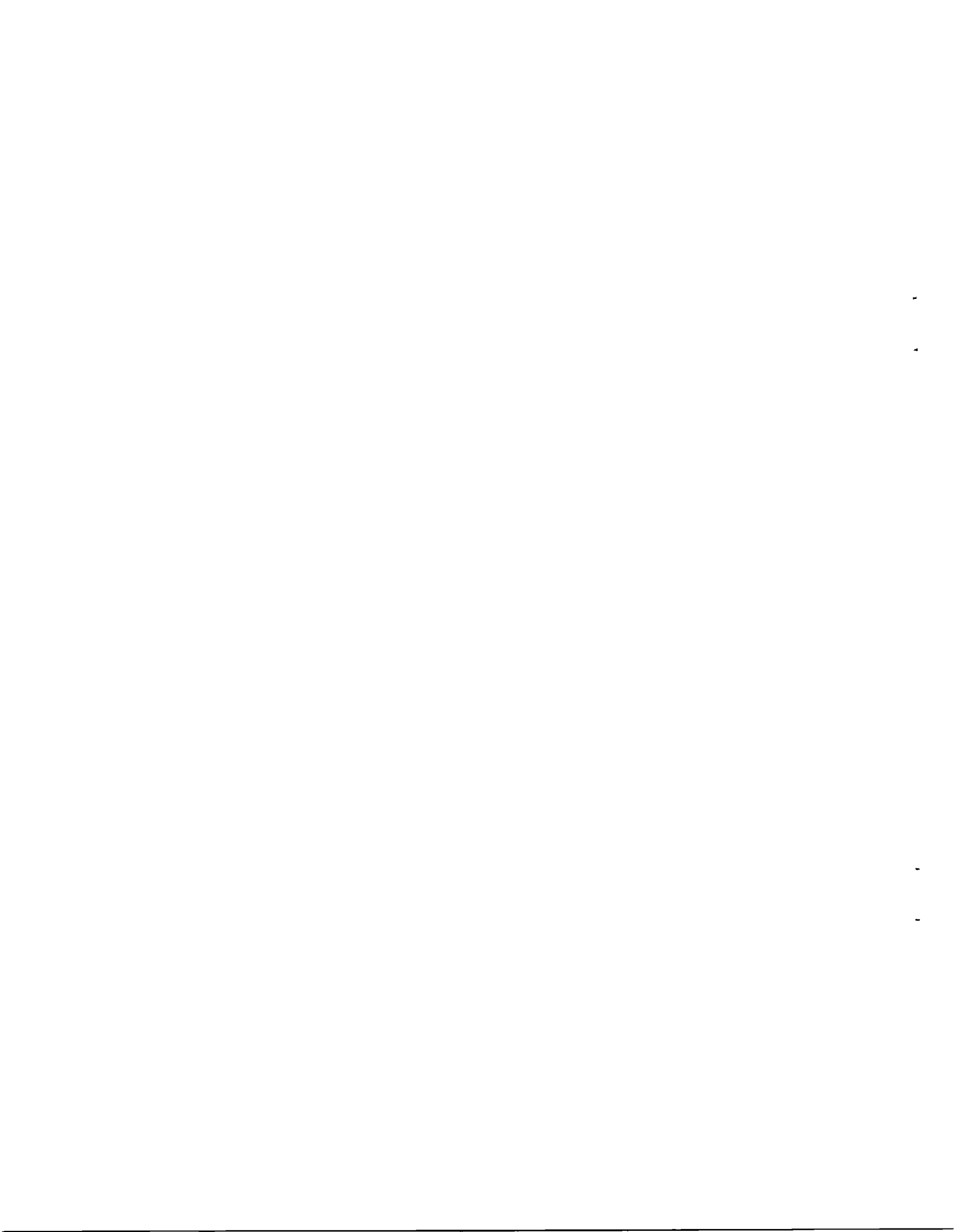
N 80 -20230

TABLE OF CONTENTS

LIST OF TABLES

LIST OF FIGURES

LIST OF FIGURES
(concluded)

NOMENCLATURE

a   Term defined in Equation 11; also, sonic velocity

A   Area

AF   Air Force

b   Intercept term in far wake shape - see Equation 9

C   Elemental concentration

c   Specific heat at constant pressure

CEC   Chemical Equilibrium Composition

CESL   Chemical Equilibrium Shear Layer

d   Diameter of probe

F   Fraction of internal species mixed with external species (similarity variable)

H   Enthalpy

HYVIS Hypersonic viscous shock layer program

m   Exponent term in far wake shape - see Equation 9

M   Mach number

$\overline{M}$ Molecular weight

MOC   Method of Characteristics

n   Term defining two-dimensional or axisymmetric flow

P   Pressure

q   Heating rate

r   Radial distance from axis of symmetry

R   Gas constant; also, Radius of probe

$Re_{\infty d}$	Reynolds number based on freestream conditions and body diameter
T	Temperature
u, U	Velocity
X	Axial distance from aft end of probe shoulder
y	Radial distance from axis of symmetry
Y	Normal coordinate (see Fig. 3)
γ	Ratio of specific heats
δ	Boundary layer thickness
$\delta*$	Boundary layer displacement thickness
ΔY	Width of mixing region
θ	Angle, momentum thickness
μ	Viscosity
ρ	Density
ψ	Stream function defined in Equation 12

Subscripts

b	Base
c	Cone
d	Diameter of probe
e	Edge of boundary layer
N	Neck
r	Reference
s	Shock, stagnation

T   Total

w   Wake, wall

∞   Freestream conditions

Section 1
INTRODUCTION

The next planetary mission that will encounter aerodynamic heating is Galileo. After more than a 3-year journey to Jupiter, the Galileo probe will enter Jupiter's atmosphere with a relative entry velocity of 48 km/sec, producing the most severe thermal environment ever encountered. In order for the probe to survive the severe aerothermal entry conditions a large portion of the probe's weight must be dedicated to the thermal protection system. Design of the thermal protection system must rely on analytical predictions since the entry thermal environment cannot be duplicated in any existing ground test facility.

The thrust of the current work is focused on the probe's wake flowfield. The wake produced by the probe is highly energetic yielding both convective and radiative heating inputs to the base of the probe. In order to calculate the radiative heating to the base region of the Jovian probe, the entire wake flowfield must be defined. This study addresses the development, improvement, and use of engineering tools for calculating the probe's wake flowfield.

The current study is an extension of previous work (Ref. 1)

1

and includes several calculation improvements as well as development of flowfields for three cases. The improvements consisted of developing a shoulder expansion code, calculating the near wake recirculation zone pressure distribution and improving the recirculation zone model. Flowfields for three entry conditions were calculated and include temperature, pressure and elemental species concentrations. These flowfields extend radially for 2.5 body radii and axially for 7.0 body radii. Section 2 of this report describes the math model used in the calculations. Section 3 provides a description of the results, and this is followed by conclusions and recommendations in Section 4.

Section 2
WAKE FLOWFIELD MODEL

The objectives of this study required the improvement and implementation of an engineering model for the Jovian probe wake flowfield. The basis of the model was developed by Engel in Ref. 1 and is shown schematically in Fig. 1. The gas state properties and the component flowfield models are discussed in detail in the following subsections. The results of applying the models to three Jovian entry conditions are presented in Section 3.

2.1 Thermodynamics

Equilibrium thermodynamic properties were used throughout this study. The curve fit coefficients for heat capacity, enthalpy and entropy were obtained from Moss (Private communications from James Moss, NASA Langley Research Center, Hampton, Virginia) for use in the chemical equilibrium composition (CEC) program (Ref. 2). Two ranges of thermodynamic property curve fits were used (1000 K to 6000 K and 6000 K to 16000 K). The CEC program determines the equilibrium composition of a gas mixture by minimization of Gibbs free energy.

The three flight cases analyzed during this study are specified in Table 1. Case 4 and 5 are documented in Ref. 3 and Case

3

3b was obtained from Moss (Private Communications from James Moss, NASA Langley, Hampton, Virginia). Computer printout from the HYVIS program (Ref. 3) were obtained for all three cases. Thermodynamic property output from the Langley HYVIS program were compared with the use of the CEC program in this study. These results are shown in Tables 2a, b and c for Cases 3b, 4 and 5 respectively. The temperature, pressure and elemental composition were specified and all other properties were computed by the CEC program. The results are for three shock layer conditions and are in excellent agreement for all variables.

The CEC program was used to calculate thermodynamic property information for the flowfield math models used in the wake. To accomplish this several options were used:

RKT - Constant entropy expansion from specified total
      conditions
T,P - Specified temperature and pressure
H,P - Specified enthalpy and pressure

Throughout the analysis six species were considered in the invis-cid flowfield and nineteen species were considered in the viscous flowfields.

2.2 Shoulder Expansion

In order to determine the initial conditions for the near wake viscous shear layer, an isentropic stream tube approximation

4

was used to calculate the boundary layer flow over the probe shoulder. The computational area of interest is shown in Fig. 2 and is confined by the body and outer edge of the viscous region over the probe shoulder.

The geometric relations used to determine the areas before and after expansion are shown in Fig. 3. HYVIS output for all points in the boundary layer are used along the Y-coordinate. These points are considered as stream tubes and expanded to locations along the Z-coordinate. The angle, θ_w, is the wake angle determined by the method of characteristics (MOC) solution just downstream of the shoulder. To expand the flow around the shoulder the following relations are used:

Known Upstream Conditions	Known Downstream Conditions
$\left.\begin{array}{c} Y_i \\ \rho_i \\ U_i \\ P_i \end{array}\right\}$ from HYVIS	$Z = 0$ $\tilde{P}_i$ – from MOC

Using continuity we may write:

$$\tilde{A}_{i+1} = A_{i+1} \ (\rho U)_{i+1} / (\widetilde{\rho U})_{i+1} \qquad (1)$$

To determine velocity the adiabatic perfect gas equation is used.

$$\frac{\tilde{U}^2}{2} + \frac{\gamma}{\gamma-1}\left(\frac{\tilde{P}}{\tilde{\rho}}\right) = \frac{U^2}{2} + \frac{\gamma}{\gamma-1}\left(\frac{P}{\rho}\right) \qquad (2)$$

Where the isentropic perfect gas relation for pressure and density is required.

$$\tilde{P}/P = (\tilde{\rho}/\rho)^\gamma \qquad (3)$$

5

The area relations from Fig. 3 are used to locate the stream-lines

$$A_{i+1} = \pi(2R_B+(Y_{i+1}+Y_i)\cos\theta_c)[Y_{i+1}-Y_i] \tag{4}$$

$$\tilde{A}_{i+1} = \pi(2R_B+\tilde{r}_{i+1}+\tilde{r}_i)[\tilde{r}_{i+1}-\tilde{r}_i]/\cos\theta_w \tag{5}$$

Let $\tilde{R} = R_B + \tilde{r}$ and solve for $\tilde{r}_{i+1}$

$$\tilde{A}_{i+1} = \pi(\tilde{R}_{i+1}^2-\tilde{R}_i^2)/\cos\theta_w \tag{6}$$

$$\tilde{r}_{i+1} = (\cos\theta_w \, \tilde{A}_{i+1}/\pi + \tilde{R}_i^2)^{\frac{1}{2}} - R_B \tag{7}$$

The key point in the expansion method is that the boundary layer must be expanded to the pressure defined by the MOC calculation. The pressure gradient predicted by the MOC near the wall is quite large as shown in Fig. 4 for the cases analyzed. These profiles were imposed on the viscous layer and yield realistic viscous edge conditions after expansion as shown in Fig. 5. The theoretical edge locations are in reasonable agreement with the experimental data from Park, (unpublished data from NASA AMES). However, the ablation rate for the ballistic range test of Park are unknown and initial flow conditions are different.

2.3 Inviscid Near and Far Wakes

The axisymmetric methods of characteristic (MOC) code of Ref. 4 as modified in Ref. 1 was used to calculate the flow properties of all the inviscid regions shown in Fig. 1. The code operates with entropy and Mach number as independent thermodynamic variables for a constant total enthalpy. The code for

6

the Jovian probe problem uses thirty velocities at each of the thirty entropy cuts. The entropy and velocity values were selected for each case considered. The MOC code was modified to provide a summary print of flow properties along the shock, the body surface and along any free boundary.

The probe's forebody was modeled as an equivalent cone. The forebody angle, θ_c , was altered to obtain an approximate match of post shock value with those of the HYVIS output. The forebody was followed by a short cylindrical section (probe shoulder). The cylindrical section was followed by a constant pressure free boundary. The base pressure correlation shown in Fig. 6 from Ref. 1 was used to establish the pressure level. The pressure values for the cases previously studied (Ref. 1) along with the values for the current cases are shown in Fig. 6. The lower boundary correlation was used to get the neck location within the neck location bounds developed in Ref. 1. These boundaries are:
                    Neck Location

$X/R = 2.8 \pm 0.4$ 　　　　　　　　　　　　　　　　　(8)

$r/R = 0.4 \pm 0.2$

        Downstream of Neck

$r/R = b (X/R)^m$ 　　　　　　　　　　　　　　　　　(9)

$m = 0.25 \pm 0.05$

The preceeding relations were based on thin boundary layer wind tunnel data. In the current problem a blown boundary layer exists which significantly alters the effective body geometry.

Consequently, an effective body radius which extends to the outer streamline of the viscous layer, see Fig. 5, was used to replace the body radius, R, in Eq. 8 and 9. This permitted obtaining consistent neck locations from Eq. 8 and 9 and from the MOC using the pressure correlation.

The far field inviscid wake started with initial conditions from the near wake calculation along the vertical dashed line shown in Fig. 1. The MOC treated the far viscous wake as a solid boundary defined by Eq. 9. The wake shock was calculated as part of the overall MOC solution. Calculations were made from the wake neck to $X/R = 7$.

The results from the MOC calculation are put on tape and are arranged along characteristic lines in cylindrical coordinates. A program was written to arrange the data in uniform radial increments at specified axial values. This program called JUGGLE also permits translation of coordinates from those used by the MOC to those desired for final data usage. The JUGGLE program was used on both the near and far inviscid wakes.

2.4 Viscous Near and Far Wakes

The near and far viscous wakes were calculated using a modified form of the computer program documented in Ref. 6. The

basic features of the program and its current application are described below.

The conservation equations for two dimensional or axisymmetric viscous mixing flow were written in terms of stream functions. An explicit finite diffrence equation was constructed for the axial momentum equation to evaluate velocity. The axial momentum equation is:

$$\frac{\partial u}{\partial x} = -\frac{1}{\rho u}\frac{dp}{dx} + \frac{1}{\psi^n}\frac{\partial}{\partial \psi}\left(a\,\frac{\partial u}{\partial \psi}\right) \tag{10}$$

where $\quad a = \mu\rho u y^{2n}/\psi^n \tag{11}$

and $\quad \psi^n \partial \psi/\partial y = \rho u y^n \tag{12}$

The term n is 0 for two-dimensional flow and 1 for axisymmetric flow. The resultant velocity values are applied in a similarity procedure to determine the degree of mixing. The degree of mixing is calculated using

$$F = \frac{U_e - U}{U_e - U_r} \tag{13}$$

In the current application, F represents the fraction of ablation products mixed with the external H_2 and He species and the nondimensional static enthalpy level. The similarity approximation can be assessed in terms of the HYVIS output at aft end of the forebody conical section (station 17). Results for the three

9

cases analyzed are shown in Fig. 7 and indicate that the similarity approximation provides a reasonable set of initial conditions for the viscous near wake.

The temperature of the mixed composition is then determined under the restraint of chemical equilibrium conditions. The velocity, temperature and other properties are located in the physical plane by an inverse transformation from the stream function plane.

The eddy viscosity model used in this study is a Prandtl-like model for compressible flow:

$$\mu = \frac{(\Delta y + \delta^*_{initial})}{900} \, | \, (\rho U)_{max} - (\rho U)_{min} \, | \, + 10^{-4} \qquad (14)$$

Other models were examined but were found to yield more rapid spreading than the observed viscous wake boundaries would indicate is realistic or no significant difference from the preceeding model.

The chemical equilibrium shear layer (CESL) program was used to calculate the near wake and far wake viscous areas. Both near and far wake calculations required special handling as described below.

The initial conditions for the near viscous wake was provided by the shoulder expansion code described in Subsection 2.2. The key concept used in obtaining a realistic expansion of the viscous layer was to superimpose the pressures determined from the MOC calculation. This same concept was extended to the outer portion of the viscous near wake as schematically shown in Fig. 2. An example of the pressure profiles derived from MOC calculations for Case 3b is shown in Fig. 8. The outer edge of the shear layer is also shown in Fig. 8 and illustrates the extent to which the viscous layer is modified by the imposed MOC pressure field.

The second important concept used in developing the near viscous wake was specifying the outer wake streamline location. This method eliminates the need to transform two dimensional solutions as done by Balakrishnan and Chu (Ref. 7). It properly accounts for the axisymmetric convergence of the flow. Further, the recompression pressure in the near wake is calculated as part of the solution. This type of approach is necessary since the shear layer is not thin compared to any dimension of the body or wake. In order to specify its physical location in the inner region, pressure must rise to accommodate the area being restricted. Thus, an axially varying constant-radial-pressure distribution is calculated. A forward integration from shoulder to wake neck region is made and a neck pressure is calculated. This

11

pressure is compared with the MOC predicted pressure. If they are not equal, the neck radius is changed and a new integration is begun.

Experimental and theoretical pressure distributions for turbulent wakes were examined to verify the expected trends. Figure 9 from Ref. 8 shows the pressure distribution for a two-dimensional case. Note that there is no constant pressure region in the data. Figures 10 and 11 from Ref. 9 show pressure distributions for axisymmetric turbulent wakes. Figure 10 is a comparison of experimental and theoretical pressures along the axis of symmetry. Both theory and data are for a cylindrical forebody. Peak pressure on these graphs and the wake neck occur at the same axial location. The theoretical results given in Fig. 11 indicate that a thick initial boundary layer thickness, δ_1, yields a very short constant pressure region.

In the present problem we have both a large δ_1 and a high expansion angle. The expansion angle is twice that of Fig. 9. Thus, no significant constant pressure region is expected. The results shown in Section 3 from the current model appear consistent with the available data and expected trends.

The far wake calculations were made with an axial pressure and corresponding edge condition variation predicted by the MOC

results. These calculations were made with axisymmetric equations without boundary location constraints. Initial conditions for the far wake were taken directly from the near wake neck location results.

2.5 Recirculation Zone

Defining the recirculation zone properties for the Jovian probe presents a rather unique base flow problem. Several aspects of this problem make it unique. First, very little experimental work has been done on turbulent wakes of large angle cones. Secondly, most experimental and theoretical wake studies have been done on thin boundary layers and not blown boundary layers as exhibited by the Jovian probe. Thirdly, few studies have addressed determining the recirculation zone enthalpy level. Fourth, high Mach number data for turbulent wakes are scarce. Finally, finding information on axisymmetric turbulent wakes which contain more than one of these aspects is rare.

In order to determine the enthalpy and concentration levels in the recirculation zone, a physical and resulting math model must be adopted. Figure 12 provides schematics for five physical models examined during the course of this study. Model 1 has a closed dividing streamline and is the model usually found in the literature. The model assumes steady state flow with the mass in

the recirculation zone constant. Problems were found with using Model 1 for the current work. First, since the mass in the recirculation zone cannot be exchanged with the external shear layer, cannot be determined. Secondly, if a steady state energy balance is made at the boundaries of the zone in Model 1, unrealistic results are obtained. If the body is assumed adiabatic, the recirculation zone total enthalpy is the freestream total enthalpy. This implies that the forebody massive ablation provides no protection to the base. If the body is nonadiabatic then the energy transferred across the dividing streamline is transferred to the body. Using this assumption the enthalpy level cannot be determined. Based on the foregoing reasons Model 1 was rejected.

Models 2 and 3 are similar in that one end of the dividing streamline is open to mass flow and steady flow is assumed. Since Model 2 would lead to an accumulation of mass and Model 3 a depletion of mass within the recirculation zone, both models were rejected.

Model 4 assumes steady flow and an open recirculation zone in which some mass from the boundary layer is captured and the same amount is allowed to exit at the wake neck. The recirculation zone is like a stirred reactor with a constant mass input and output. The mechanisms which would allow both a capturing and escape of mass could not be identified from the literature.

14

If this process is real, a capturing model for flow over the shoulder would require development.

The literature on separated and wake flows by Chilcott (Ref. 10) and Charwat et. al. (Ref. 11) suggest that a pulsating mass exchange process exists and the degree to which this behavior dominates is geometry dependent. Using this concept, Model 5 was developed. The dividing streamline is closed at the shoulder and periodically open at the wake neck. The opening process loses mass and the closing process pumps mass into the recirculation zone. Charwat et. al. (Ref. 11) points out that even for cavity type flows neither the "conduction" model, corresponding to Model 1, nor the mass exchange model are sufficiently complete. In the current problem, effects of Model 1, 4 and 5 are thought to contribute to the recirculation zone properties. The conduction across the dividing streamline, and the mass exchange mechanisms of Models 4 and 5 determine the recirculation zone enthalpy. The mass exchange mechanisms of Models 4 and/or 5 determine the elemental composition within the recirculation zone.

Since development of a steady state model based on global energy and mass balances do not appear feasible and correct, an empirical approach was taken. Experimental data exist for the recirculation zone temperatures of nonablating bodies. Huber and Hunt (Ref. 12) compiled data to compare with the Apollo shape.

15

These data are shown in Fig. 13 where temperature was replaced by enthalpy. Turbulent flow data corresponding to $Re_{\infty d} \geq 10^6$ for the Apollo shape was selected to best represent the Jovian probe. Wall enthalpy does not Bsignificantly influence the recirculation zone enthalpy since H_w/H_T=0.030 to 0.039 for the cases analyzed. A value of $(H_b-H_w)/(H_T-H_w) = 0.5$ was selected as a conservative estimate for the design application herein. An improved estimate and model awaits test data for hypersonic blunt cones with massive forebody blowing.

Section 3
RESULTS

This section presents observations about the three wake flowfields calculated and presents the format in which the flowfields were recorded for radiation analysis work.

3.1 Flowfield Distributions

The analytical methods described in Section 2.0 were used to calculate three flowfields corresponding to three possible Jovian probe entry conditions. The specifying conditions for the three cases are given in Table 1. Case 3b corresponds to peak forebody heating for a cool atmosphere model with a steep entry angle. Cases 4 and 5 are for a nominal atmosphere model and nominal entry angle (Ref. 3). Case 4 corresponds to peak forebody heating in the nominal entry trajectory.

The starting location for the current flowfields is where the HYVIS program terminates at the end of the Jovian probe conical section (Station 17). It is therefore appropriate to compare the MOC solution on the conical section with the HYVIS results. MOC results are for a sharp cone whereas the HYVIS results are for a sphere-cone body. Post shock results are given in Table 3 and are found to be in good agreement. The body angle used in

the MOC calculation was larger than the actual body angle to account for effective body displacement due to massive blowing.

The post shock conditions shown in Table 3 are indicative of the relative temperature and pressure levels in the respective wakes. This point will become apparent as the results given in this section are reviewed. The post shock conditions for the forebody shock past the probe's shoulder are shown in Fig. 14. Case 3b exhibits the highest temperatures whereas Case 5 exhibits the lowest temperatures. This same trend persists throughout the near and far wake inviscid flowfields as summzrized in Fig. 15. Post wake shock conditions may be significant for Case 3b but appear somewhat benign for Case 5.

Streamline pressures and temperatures for the viscous near and far wakes are shown in Figs. 16 to 21. The external and internal viscous streamline pressures, shown in Figs. 16, 18 and 20, converge at $X/R \approx 0.5$. Between $X/R = 0$ and 0.5 large radial pressure gradients exist in the shear layer as shown in Fig. 8. This high pressure and pressure gradient region produces the high temperature levels shown in Figs. 17, 19, and 21. The models used in the previous work (Ref. 1) did not account for this pressure effect and thus did not identify this high temperature region. The rise in temperature at the neck location is a result of the wake shock. Figures 17, 19, and 21 also show the recircu-

18

lation region temperature levels. The slight rise with increas-
ing X/R is due to the axial pressure rise in the recirculation
zone which matches the inner streamline pressure.

Near wake radial profiles for the peak forebody heating con-
ditions of two trajectories are shown in Fig. 22. Pressure lev-
els and temperature levels in the recirculation region, viscous
layer and inviscid region are higher for Case 3b than for Case 4.
Mass fraction levels of carbon in the recirculation and viscous
layers are comparable for the two cases.

The nondimensional pressure distributions in the near wake
calculated using the model described in Section 2.3 are shown in
Fig. 23. The effect of massive blowing increases the boundary
layer thickness and nearly eliminates the plateau pressure region
in the near wake. This trend has been illustrated for less sev-
ere cases by Ref. 9 as shown in Fig. 11. The base pressure is
increased but only slightly by increased ablation. The calculat-
ed neck pressure for the three cases is between 2.5 and 3.3 times
the base pressure. This agrees with the data and theory of Fig.
10 and data and theoretical results presented by Wong and Chow in
Ref. 21. However, the current results are significantly differ-
ent from those presented by Park (Ref. 22).

Park in Ref. 22 assumed a base flow model like Model 1 of

Fig. 12 to establish the neck pressure. A dividing streamline velocity of 50 percent of the external velocity was assumed to stagnate and close the recirculation zone. This leads to the high neck pressures presented in Ref. 22. No explanation of how the recirculation mass fraction or enthalpy level can be estimated using the closed recirculation zone concept was given. Park estimated the neck to stagnation pressure ratio $P_N/P_S = 0.15$ for Case 4 of this report. This may be compared to the current results in Table 4. By using base heating rate correlation of Ref. 22 with the current neck pressures, the base radiative heating was estimated to be 0.925 MW/m^2 compared to the value of 19.4 MW/m^2 from Ref. 22. The actual value for Case 4 from the current analysis must await the detailed radiative calcualtions for the flowfield provided by this work. However, by using the correlation of Park the current results would appear to yield heating rates lower by a factor of 20 than results of Park's and higher by a factor of about 3 than the results from Brant and Nestler (Ref. 5).

The main uncertainty and differences between different analysis is the manner in which the recirculation region is closed. This produces different models for the recirculation zone species and enthalpy level as well as different wake neck pressure levels. All of these factors significantly affect the base heating environment. This uncertainty will most likely persist until an

20

experimental data base is available for blunt planetary probe class bodies and entry conditions.

3.2 Flowfield Format

The flowfield results for all three cases were delivered to NASA-Langley on cards. The flowfield properties were provided in nondimensional cylindrical coordinates starting at the aft end of the probes shoulder and going to $X/R = 7.0$. The card format is defined in Table 5. The flowfield for each case consists of approximately 1300 points where temperature, pressure and elemental composition is defined.

Section 4
CONCLUSIONS AND RECOMMENDATIONS

Based on the analysis and results of this study, the following conclusions are drawn.

(1)   Case 3b exhibited the highest wake temperatures and Case 5 the lowest wake temperatures.

(2)   The neck pressure was calculated to be approximately 3 times the base pressure.

(3)   The current pressure model for the outer portion of the shear layer produces a high temperature region in the shear layer for $X/R \leq 0.5$.

(4)   The recirculation zone enthalpy can be only approximated using current models and experimental data.

(5)   Large differences exist in the neck pressures used by different options to model the Jovian probe wake.

As a consequence of the information obtained in this study, the following recommendation is made.

An experimental program, for general planetary probe application, should be undertaken to establish:

(a)   The pressure distribution in the near wake both with and without massive blowing.

(b)   The elemental composition in the recirculation zone as a function of blowing rate.

(c)   The recirculation zone enthalpy as a function of blowing rate and mass injection enthalpy ratio to total enthalpy.

Section 5
REFERENCES

1. Engel, C. D., "Jovian Probe Wake Flowfield," NASA CR 159021, March 1979.

2. Gordon, S. and B. J. McBride, "Computer Program for Calculation of Complex Chemical Equilibrium Compositions, Rocket Performance, Incident and Reflected Shocks, and Chapman-Jouguet Detonations," NASA SP-273, February 1973.

3. Moss, J. N., "A Study of the Aerothermal Entry Environment for the Galileo Probe," AIAA Paper No. 79-1081, June 1979.

4. Smith, S. D. and A. W. Ratliff, "Rocket Exhaust Plume Computer Program Improvement," LMSC-HREC D162220, Lockheed Missiles and Space Company, June 1971.

5. Brant, D. N., and D. E. Nestler, "Development of an Afterbody Radiative and Convective Heating Code for Outer Planet Probes," AIAA Paper 78-862, May 1978.

6. Audeh, B. J., "Equilibrium Shear Layer Program," TM 54/20-169, Lockheed Missiles and Space Company, December 1967.

7. Balakrishnan, A. and E. Chu, "Jupiter Entry Probe Afterbody Convective Heating," AIAA Paper No. 79-0040, January 1979.

8. Wagner, Richard D. "Measured and Calculated Mean-Flow Properties of Two-Dimensional, Hypersonic, Turbulent Wake," NASA TN D-6927, Langley Research Center, Novermber 1972.

9. Mehta, Gopal K. and Warren C. Strahle, "A Theory of the Supersonic Turbulent Axisymmetric Near Wake Behind Bluff-Base Bodies," AIAA Journal, Vol. 15, No. 8, August 1977, pp. 1059-1060, backup document.

10. Chilcott, R. E., "A review of Separated and Reattaching Flows With Heat Transfer," J. Heat Mass Transfer, Vol. 10, pp. 783-797, 1967.

11. Charwat, A. F., C. F. Dewey, Jr., J. N. Roos, and J. A. Hitz, "An Investgation of Separated Flows - Part II: Flow in the Cavity and Heat Transfer," J. of the Aerospace Sciences, Vol. 28 No. 7, pp. 513-527, July 1961.

12.   Huber, P. W., and J. L. Hunt, "Reynolds Number Dependence of Apollo Near Wake Temperature," AIAA Journal, Vol. 6, No. 1, January 1968, pp. 184, 185.

13.   Weiss, R. F. and Weinbaum, S., "Hypersonic Boundary Layer Separation and the Base Flow Problem," Research Rept. 221, July 1965, Avco-Everett Research Laboratory, Everett, Mass.

14.   Todisco, A. and Pallone, A. J., "Near Wake Flow Field Measurements," AIAA Journal, Vol. 3, No. 11, November 1965, pp. 2075-2080.

15.   Zakkay, V. and Cresci, R. J., "An Experimental Investigation of the Near Wake of a Slender Cone at M_∞ = 8 and 12," AIAA Journal, Vol. 4, No. 1, January 1966, pp. 41-46.

16.   Muntz, E. P. and Softley, E. J., "A Study of Laminar Near Wakes," AIAA Journal, Vol. 4, No. 6, June 1966, pp. 961-968.

17.   Reeves, B. L. and Lees, L., "Theory of Laminar Near Wake of Blunt Bodies in Hypersonic Flow," AIAA Journal, Vol. 3, No. 11, November 1965, pp. 2061-2074.

18.   Todisco, A. and Pallone, A., "Measurements in Laminar Near Wakes," AIAA Paper 67-30, January 1967, New York.

19.   Beckwith, I. E., Bushnell, D. M., and Huffman, J. K., "Investigation of Water Injection on Models of Gemini Vehicle and Resulting Predictions for GT-3 Reentry Communications Experiment," NASA TM X-1200, March 1966.

20.   Martellucci, A., Trucco, H., and Agnone, A., "Measurements of the Turbulent Near Wake of a Cone at Mach 6," AIAA Journal, Vol. 4, No. 3, March 1966, pp. 385-391.

21.   Weng, C. H. and W. L. Chow, "Axisymmetric Supersonic Turbulent Base Pressures," AIAA Journal, Vol. 16, No. 6, pp. 553, 554, June 1978.

22.   Park, Chul, "Problems of Radiative Base Heating," AIAA/NASA Conference on Advanced Technology for Future Space Systems, Paper No. 79-0919, May 1979.

Table 1

SPECIFYING CONDITIONS

Variable	Case 3b	Case 4	Case 5
Time (sec)	85.25	111.3	113.5
Altitude (km)	93.346	126.05	115.31
Atmosphere Mass Fractions			
H_2	.641	.803	.803
He	.359	.197	.197
P_∞ (atm)	.004429	.002422	.003795
T_∞ (°K)	132.07	152.00	148.0
M_∞	46.975	43.009	38.45
V_∞ (m/sec)	37547	39284	34666

Table 2a
Case 3b
COMPARISON OF EQUILIBRIUM THERMODYNAMIC CALCULATIONS

Variable	Condition 1		Condition 2		Condition 3	
	REMTECH	Langley	REMTECH	Langley	REMTECH	Langley
P atm	12.651	12.651	7.1249	7.1249	7.436	7.436
T K	17125	17125	12999	12999	3978	3978
H cal/gm	166386.	166322.	94742	94716	5417.9	5423.9
$\bar{M}$ Mol wt	1.118	1.118	1.307	1.307	30.824	30.787
c_p cal/gm K	26.2726	-----	12.7979	-----	2.1459	------
γ	1.2215	-----	1.2480	-----	1.1076	------
a m/sec	12474.3	-----	10158.7	-----	1090.1	------
Mole Fractions						
H	.52184	.52199	.77931	.77949	.10850	.10904
H_2	.00003	.00003	.00010	.00009	.03768	.03768
H^+	.18890	.18890	.05168	.05169	------	------
He	.10016	.09999	.11723	.11704	.01757	.01752
He^+	.00009	.00009	------	------	------	------
e-	.18899	.18899	.05168	.05169	------	------
C	------	------	------	------	.00788	.00797
C_2	------	------	------	------	.01026	.01035
C_3	------	------	------	------	.17830	.17900
C_2H	------	------	------	------	.12088	.12101
C_2H_2	------	------	------	------	.02347	.02337
C_3H	------	------	------	------	.14328	.14295
C_4H	------	------	------	------	.23732	.23634
CO	------	------	------	------	.11486	.11474

Condition

1 - Post Shock (Stagnation Point)
2 - Post Shock (Station 17) ⎫
3 - Wall (Station 17) ⎬ At aft end of forebody conical section

Table 2b

Case 4

COMPARISON OF EQUILIBRIUM THERMODYNAMIC CALCULATIONS

Variable	Condition 1		Condition 2		Condition 3	
	REMTECH	Langley	REMTECH	Langley	REMTECH	Langley
P atm	6.008	6.008	3.356	3.356	3.469	3.469
T °K	15742	15742	11822	11822	3878	3878
H cal/gm	182219.8	182150.0	102858.3	102838.9	5510.9	5506.5
$\bar{M}$ Mol wt	0.972	0.972	1.137	1.137	29.986	30.009
c_p cal/gmK	32.7970	----	13.3459	----	2.4762	----
γ	1.2105	----	1.2560	----	1.1071	----
a m/sec	12767.6	----	10421.4	----	1091.0	----
Mole Fractions						
H	0.59623	.59845	0.86674	.86683	0.13143	.13097
H_2	0.00002	.00002	0.00009	.00009	0.03700	.03703
H^+	0.17794	.17792	0.03860	.03861	----	----
He	0.04783	.04776	0.05596	.05587	0.00742	.00743
He^+	0.00002	.00002	----	----	----	----
e-	0.17796	.17794	0.03860	.03861	----	----
C	----	----	----	----	0.00968	.00960
C_2	----	----	----	----	0.01156	.01150
C_3	----	----	----	----	0.20350	.20291
C_2H	----	----	----	----	0.12161	.12157
C_2H_2	----	----	----	----	0.01922	.01930
C_3H	----	----	----	----	0.13837	.13863
C_4H	----	----	----	----	0.20833	.20905
CO	----	----	----	----	0.11187	.11199

Condition

1 - Post Shock (Stagnation Point)
2 - Post Shock (Station 17)
3 - Wall (Station 17)

27

Table 2c

Case 5

COMPARISON OF EQUILIBRIUM THERMODYNAMIC CALCULATIONS

Variable	Condition 1		Condition 2		Condition 3	
	REMTECH	Langley	REMTECH	Langley	REMTECH	Langley
P atm	7.447	7.447	4.105	4.105	4.228	4.228
T °K	14475	14475	8839	8839	3765	3765
H cal/gm	141561.3	141531.1	77711.9	77700.0	5498.5	5503.9
$\bar{M}$ Mol wt	1.059	1.059	1.180	1.180	23.600	23.579
c_p cal/gmK	22.929	-----	5.2033	------	2.4672	-------
γ	1.2187	-----	1.5199	------	1.1163	-------
a m/sec	11766.9	-----	9729.8	------	1216.9	-------
Mole Fractions						
H	.73960	.73967	.93601	.93611	.18329	.18400
H_2	.00006	.00006	.00061	.00061	.13453	.13427
H^+	.10410	.10411	.00265	.00265	------	------
He	.05214	.05205	.05809	.05799	.03299	.03291
He^+	------	-----	------		------	------
e-	.10410	.10411	.00265	.00265	------	------
C					.00396	.00399
C_2					.00412	.00416
C_3					.07108	.07146
C_2H					.12677	.12690
C_2H_2					.05255	.05229
C_3H					.13260	.13242
C_4H					.17211	.17165
CO					.08599	.08593

Condition 1 - Post Shock (Stagnation Point)
　　　　　　　2 - Post Shock (Station 17)
　　　　　　　3 - Wall (Station 17)

Table 3

COMPARISON OF CONE SECTION POST-SHOCK CONDITIONS

Variable	Units	Case 3b		Case 4		Case 5	
		REMTECH	LANGLEY Sta. 17	REMTECH	LANGLEY Sta. 17	REMTECH	LANGLEY Sta. 17
T	K	13,044	12,999	11,908	11,822	8994	8839
P	atm	7.241	7.125	3.432	3.356	4.213	4.105
Avg. Mol. Weight	---	1.306	1.3074	1.1345	1.137	1.179	1.180
$\theta_s - \theta_c$ (Blowing)	deg.	3.91	4.18	3.733	3.88	3.47	2.902
θ_c	deg.	46	45	46	45	45.4	45

Table 4

BASE PRESSURES SUMMARY AND BASE RADIATIVE HEATING ESTIMATES

Case	P_s (atm)	P_N (atm)	P_N/P_s	P_N/P_b	q_b/q_s (1)	q_s (2) (MW/m^2)	q_b (3) (MW/m^2)
3b	12.651	.2721	.0215	3.32	.00757	451.9	3.42
4	6.008	.0964	.0160	2.52	.00488	189.5	0.925
5	7.447	.1278	.0168	2.59	.00520	166.3	0.605

Notes (1) $q_b/q_s = 2.4 \, (P_N/P_s)^{1.5}$ from Park (Ref. 22)

(2) q_s = stagnation coupled ablation radiative heating from HYVIS

(3) q_b = base radiative estimate using (1) and (2)

Table 5

CARD FORMAT

Column	Format	Variable
1 - 10	F10.6	X/R, nondimensional axial distance
11 - 20	F10.6	r/R, nondimensional radial distance
21 - 30	F10.4	Static temperature (°K)
31 - 40	F10.8	Static pressure (atm)
41 - 50	F10.7	Mass fraction of hydrogen
51 - 60	F10.7	Mass fraction of helium
61 - 70	F10.7	Mass fraction of carbon
71 - 80	F10.7	Mass fraction of oxygen
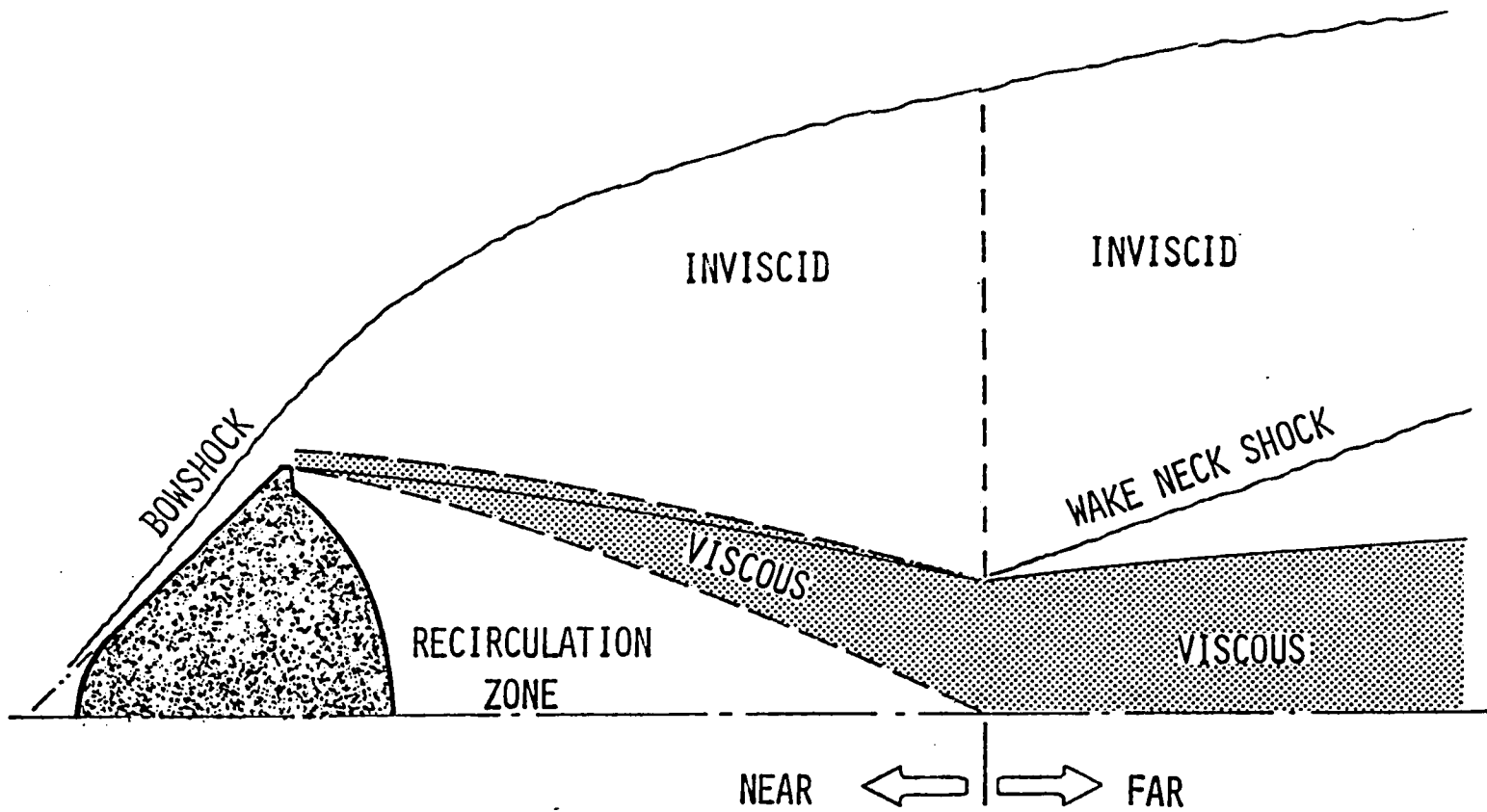
Fig. 1 Computational Regions for the Jovian Probe Wake Flowfield
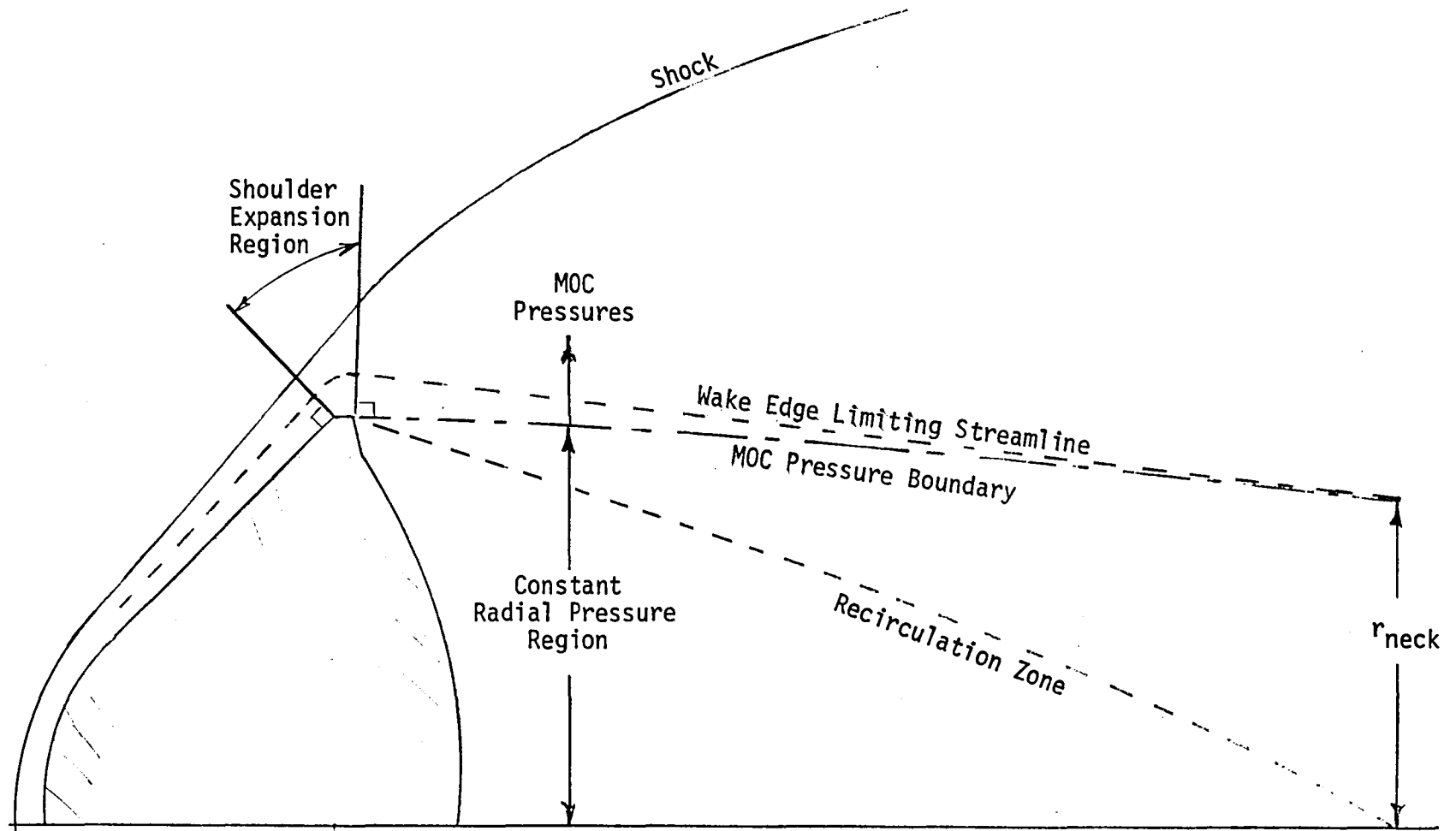
Fig. 2   Near Wake Calculation Regions
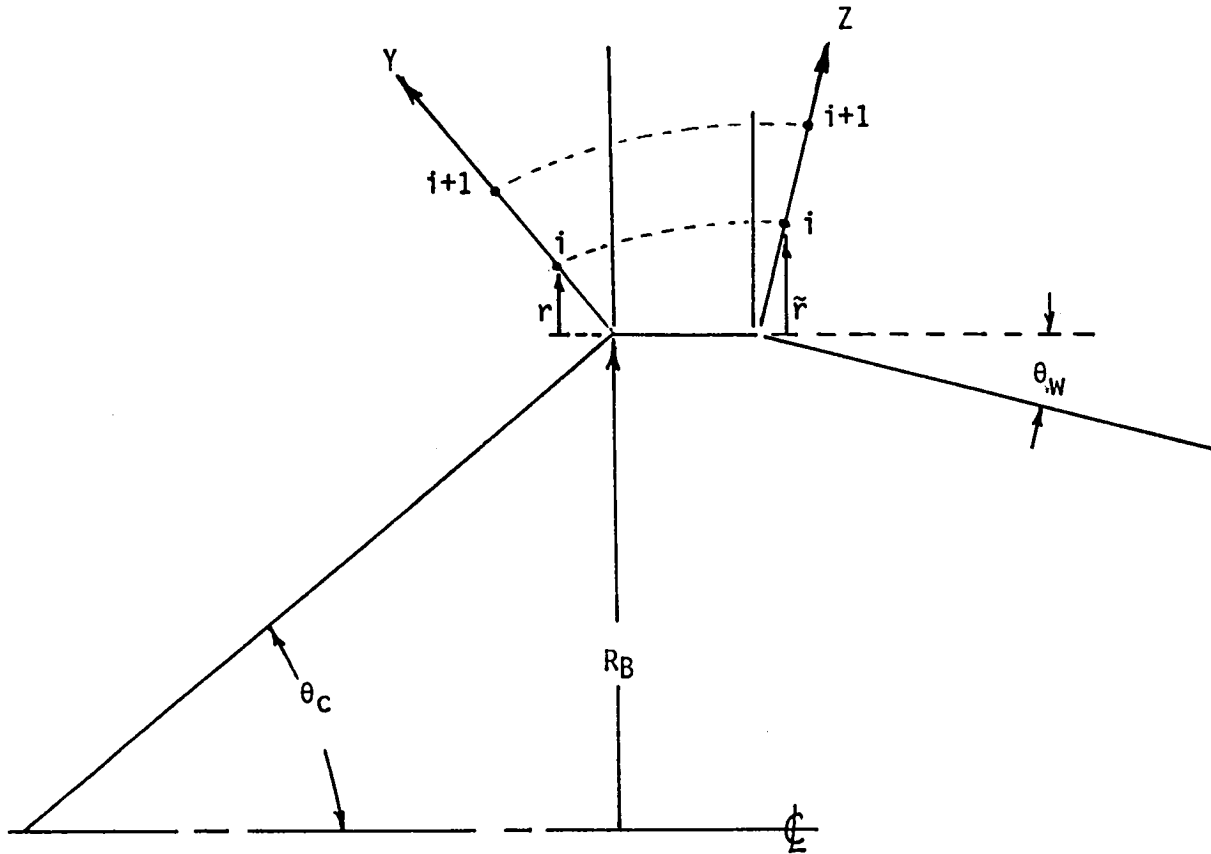
Cone Frustum Areas

$$A_{i+1} = \pi \, ((r_{i+1}+R_B) + (r_i+R_B))[Y_{i+1} - Y_i]$$

$$\tilde{A}_{i+1} = \pi \, ((\tilde{r}_{i+1}+R_B) + (\tilde{r}_i+R_B))[Z_{i+1}-Z_i]$$

$$r = Y \cos\theta_c$$

$$\tilde{r} = Z \cos\theta_w$$

Therefore

$$A_{i+1} = \pi \, (2R_B+(Y_{i+1}+Y_i)\cos\theta_c)[Y_{i+1}-Y_i]$$

$$\tilde{A}_{i+1} = \pi \, (2R_B+\tilde{r}_{i+1}+\tilde{r}_i)[\tilde{r}_{i+1}-\tilde{r}_i]/\cos\theta_w$$

Fig. 3   Shoulder Expansion Geometry
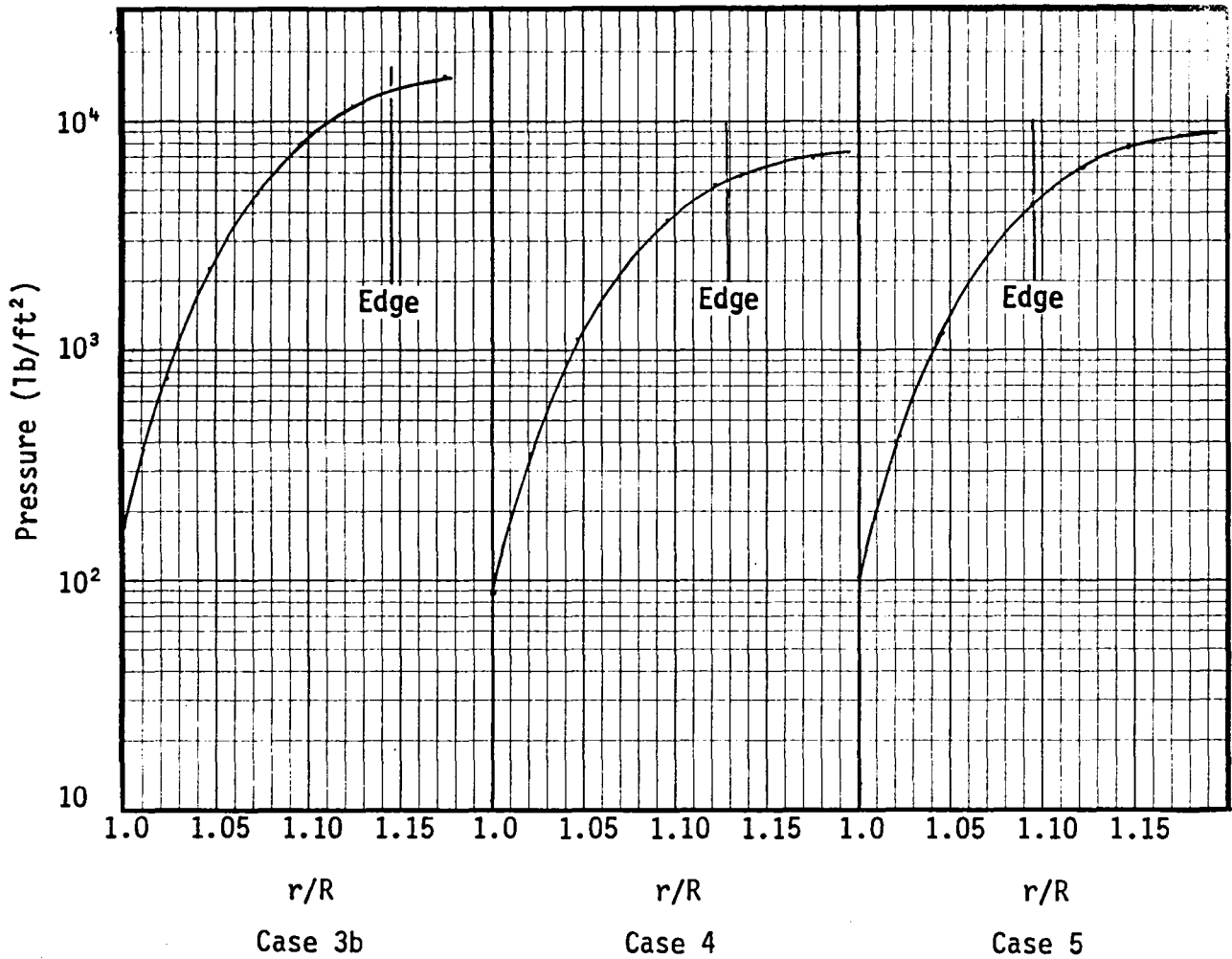
Fig. 4   Shoulder Aft Position Pressure Profiles
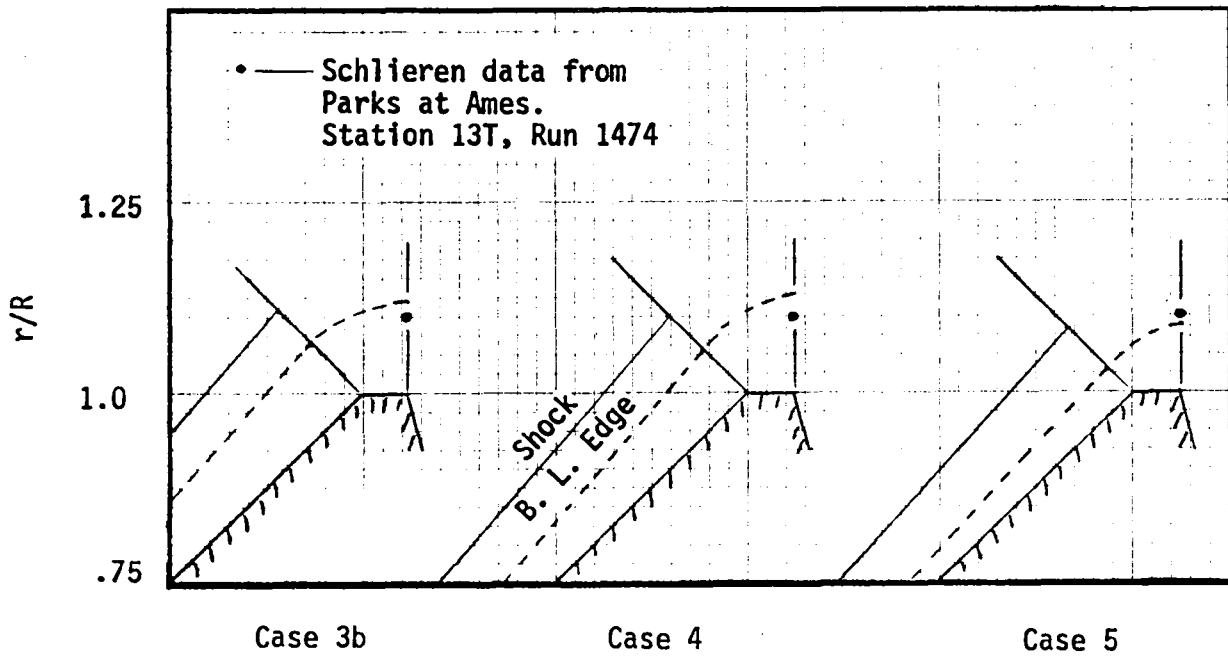
Fig. 5   Boundary Edge Geometries Over the Probes Shoulder
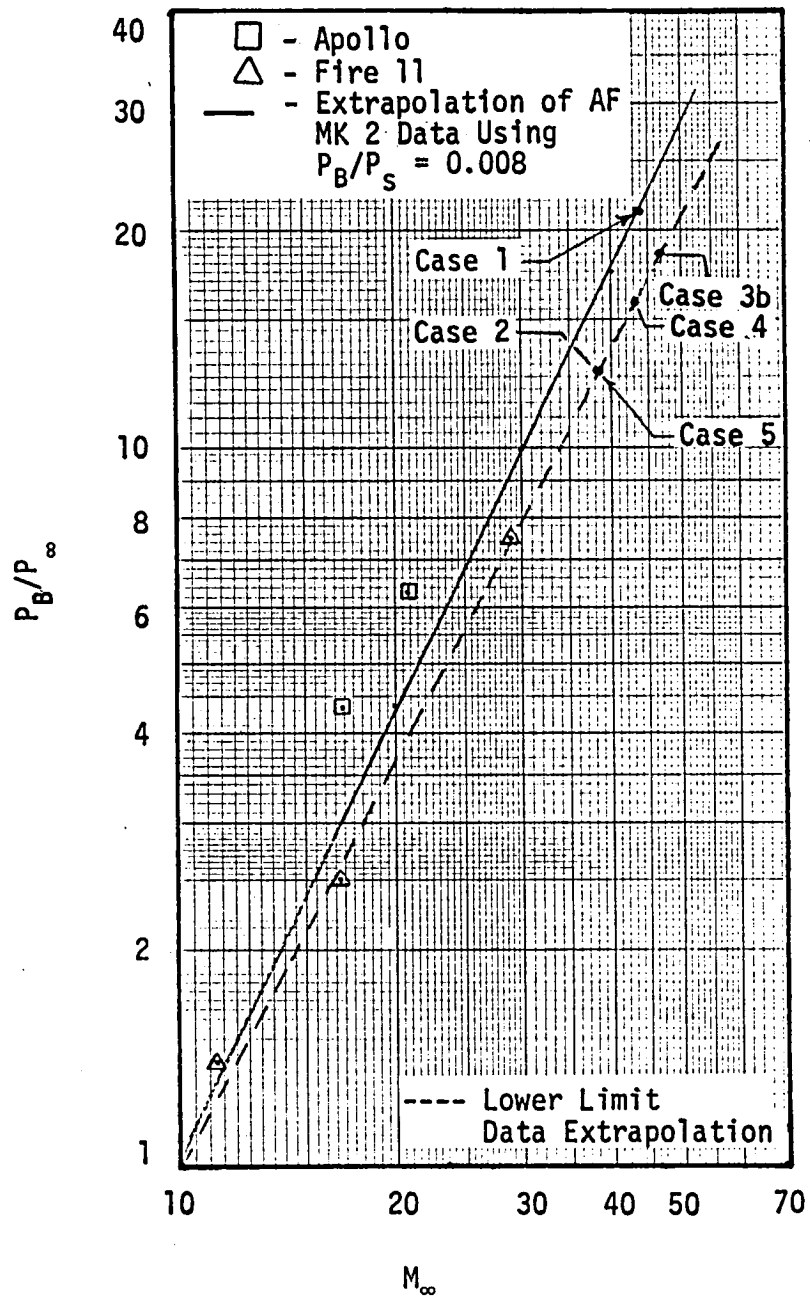
Fig. 6   Turbulent Base Pressure Correlation for Planetary
          Entry Systems (From Brant and Nestler, Ref. 5)
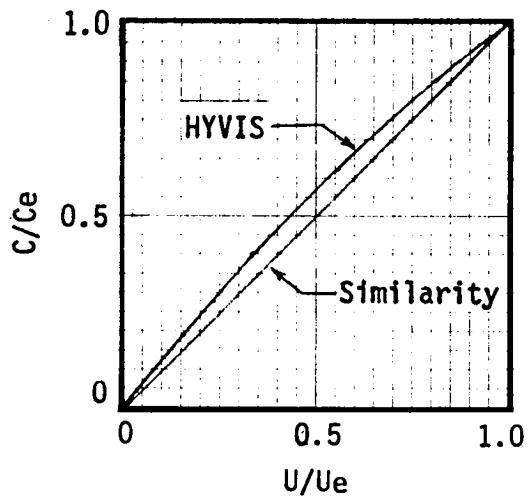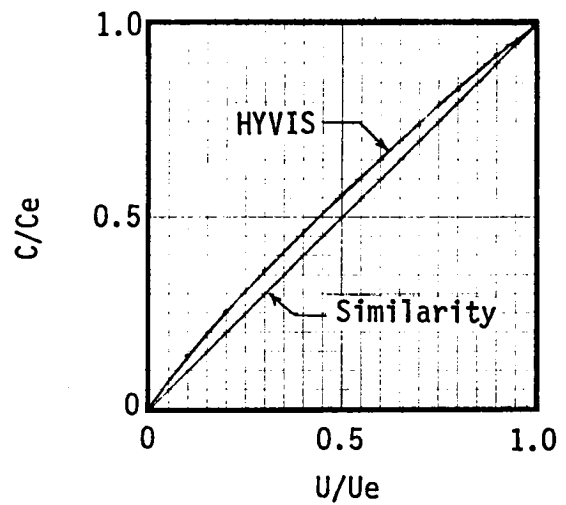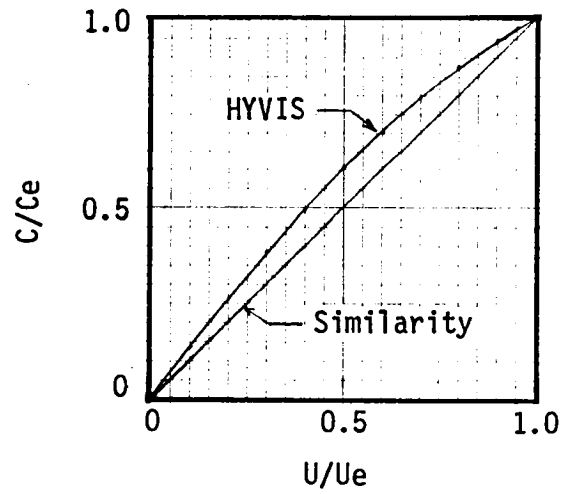
Fig. 7   Comparison of the Similarity Approximation With HYVIS
         Results at Station 17.
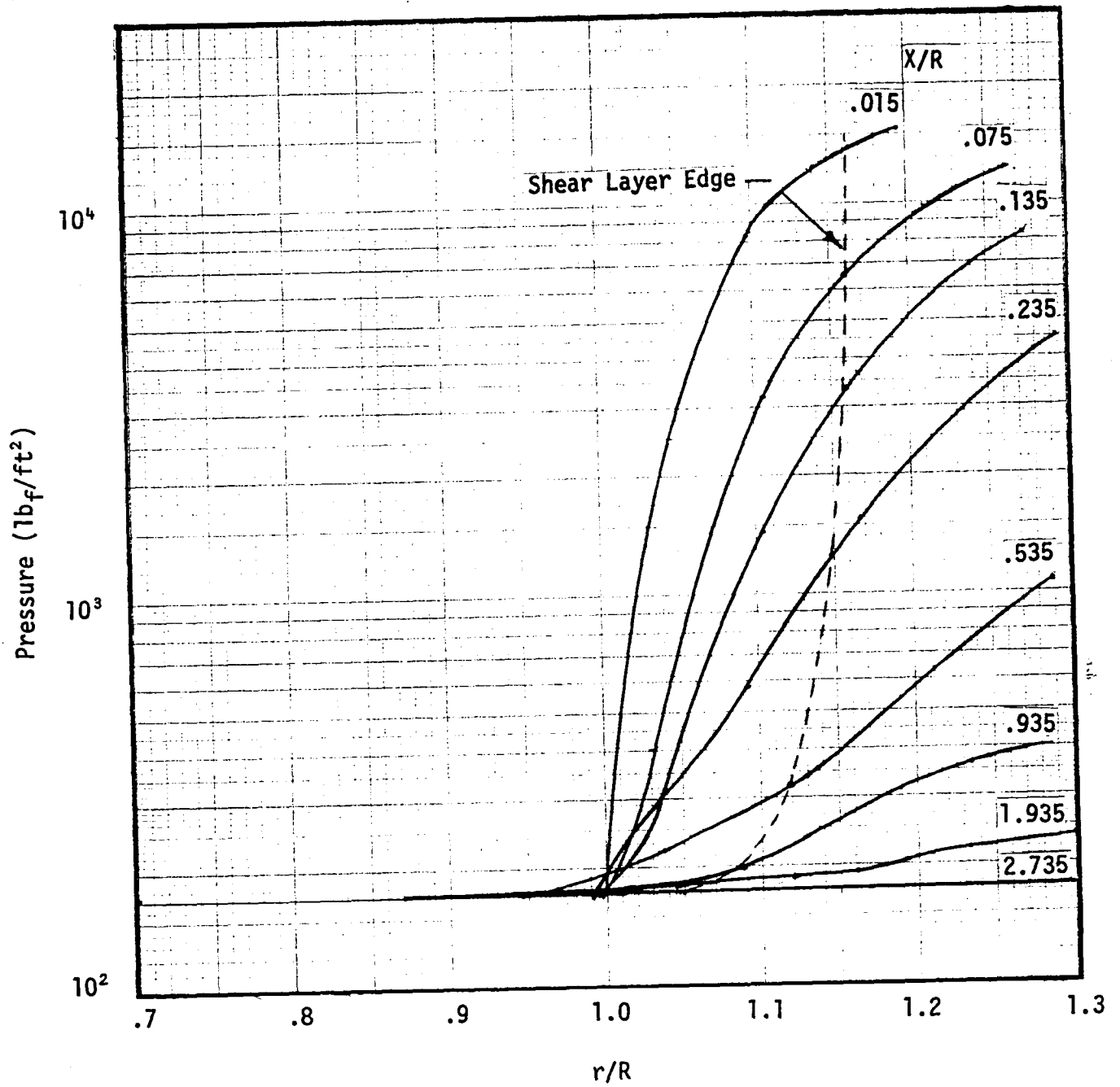
Fig. 8   Case 3b MOC Radial Pressure Profiles
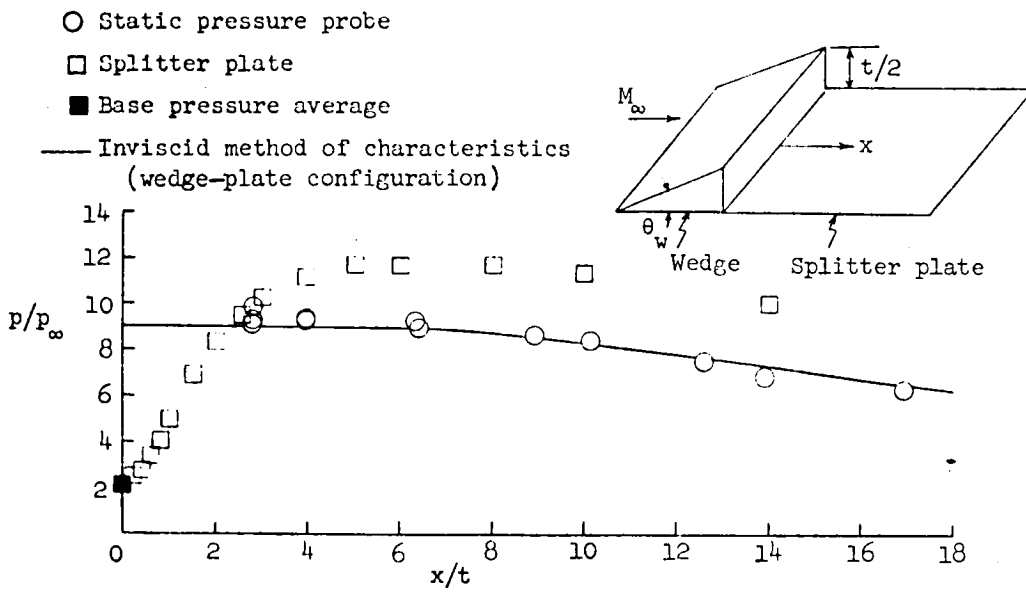
Fig. 9 Two-Dimensional Turbulent Wake Spliter Plate Pressure Distribution (M_∞ = 20.4, Re_∞ = 3.4x10^5, θ_W=22.5°) [From Wagner (Ref. 8)]
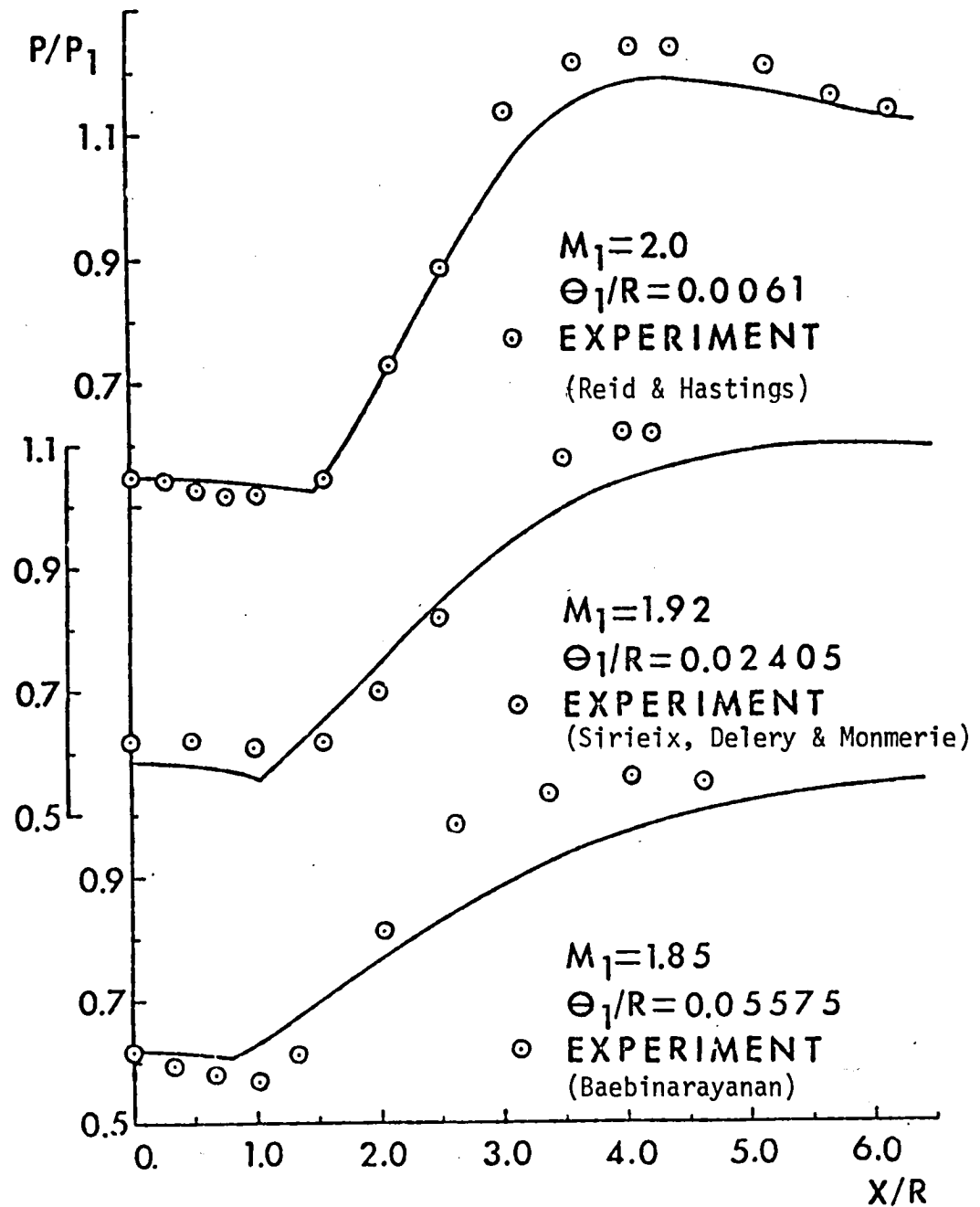
Fig. 10 Comparison of Experimental and Theoretical Turbulent
Axisymmetric Wake Centerline Pressure Distributions
(From Mehta and Strahle, Ref. 9)

39
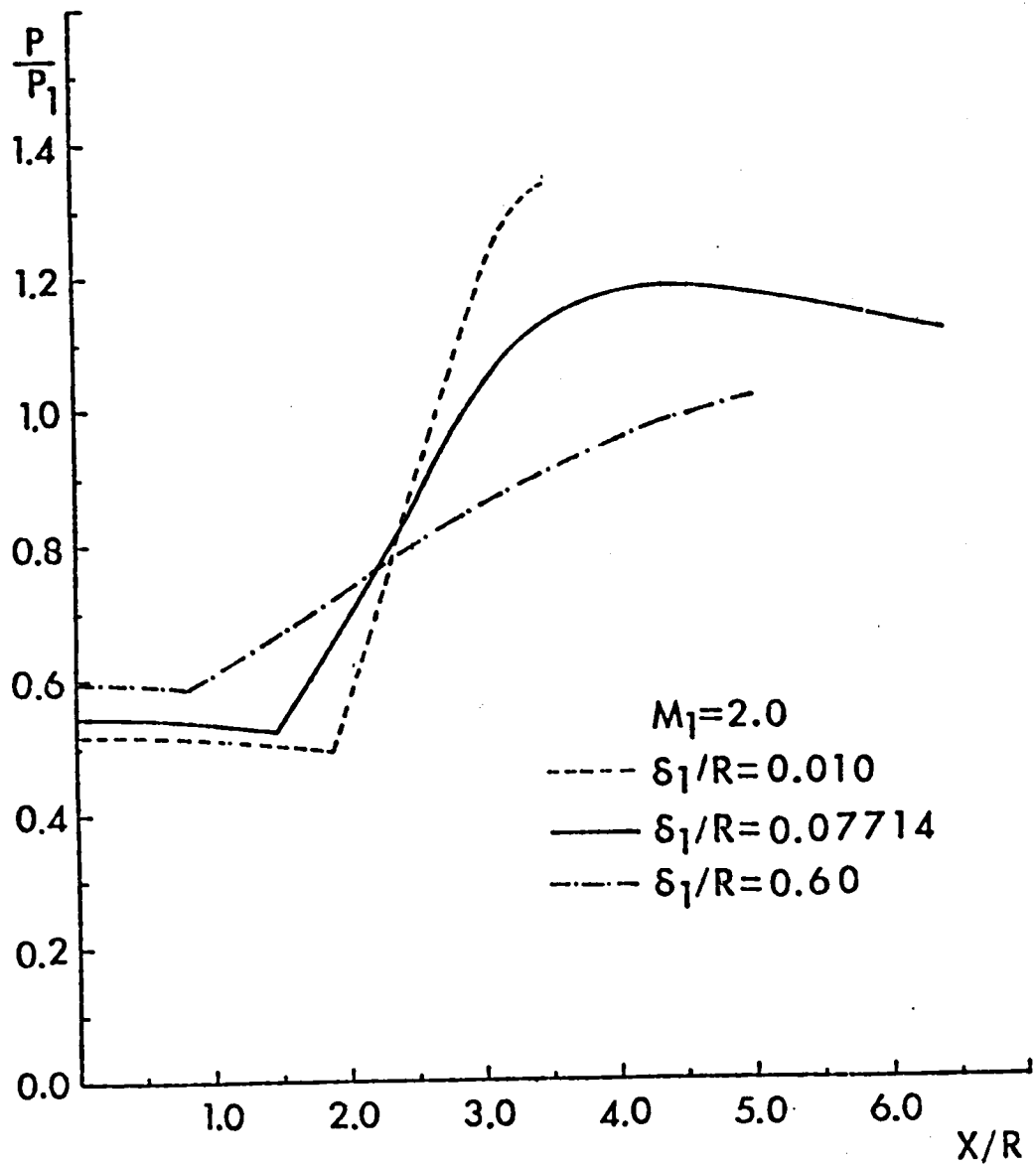
Fig. 11   Comparison of Theoretical Turbulent Axisymmetric Wake
Centerline Distributions for Different Initial Boundary
Layer Thicknesses (From Mehta and Strahle, Ref. 9)

δ — closed   Model 1

— Dividing Streamline

Recirculation Zone

—Closed

δ — open   Model 2

—Closed

δ — closed   Model 3

—Open

δ — open   Model 4

—Open

δ — closed   Model 5

—Pulsating
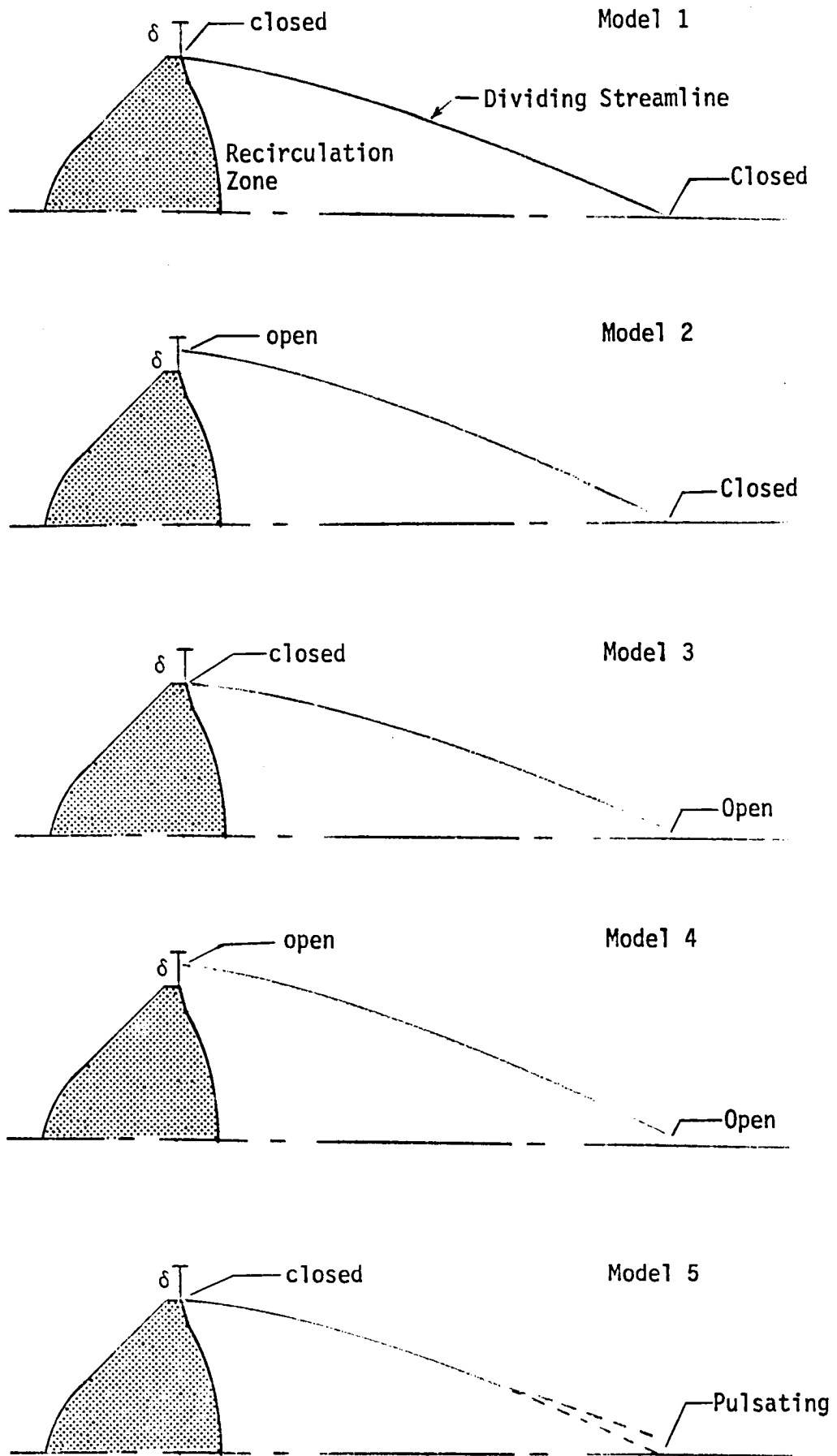
Fig. 12   Recirculation Zone Models

41

Fig. 13   Comparison of Reynolds Number Dependence on Near-Wake
           Enthalpy   (From Ref. 12)
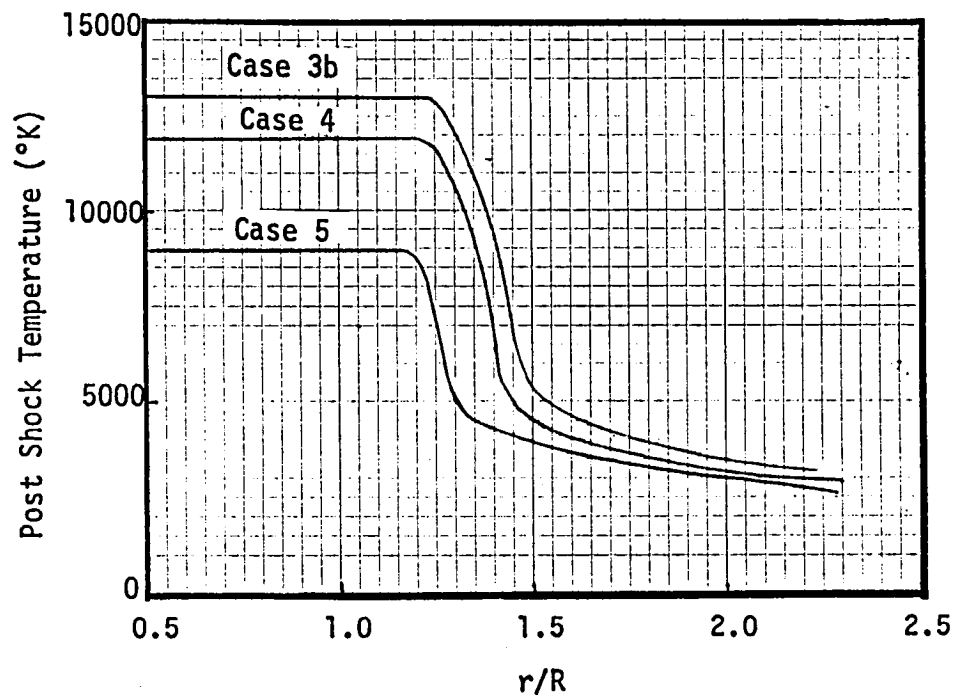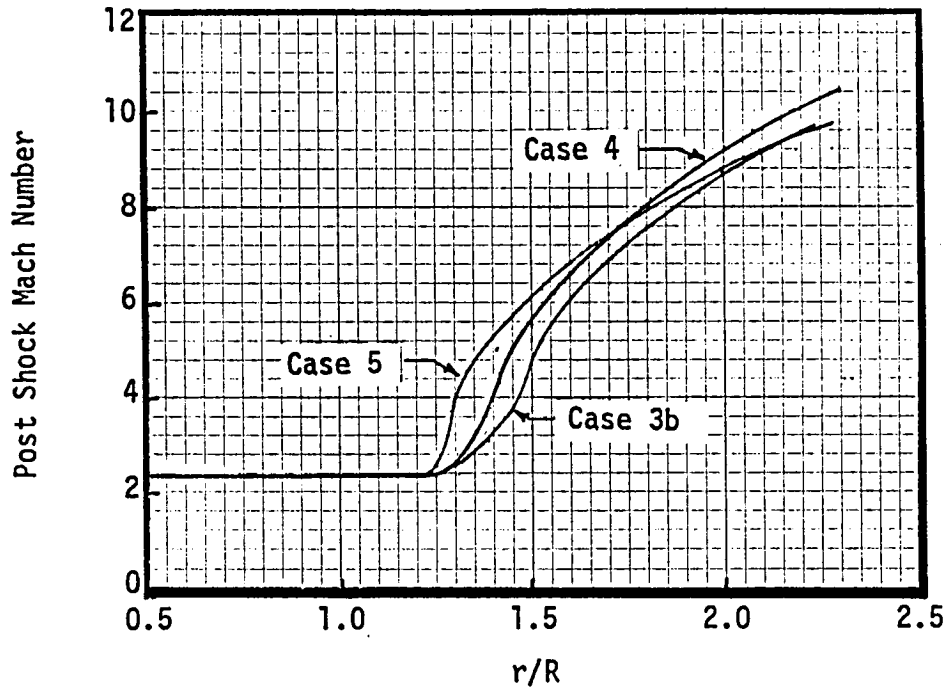
Fig. 14 Post Forebody Shock Conditions

(VALUES IN ITALICS ARE P/P_∞)
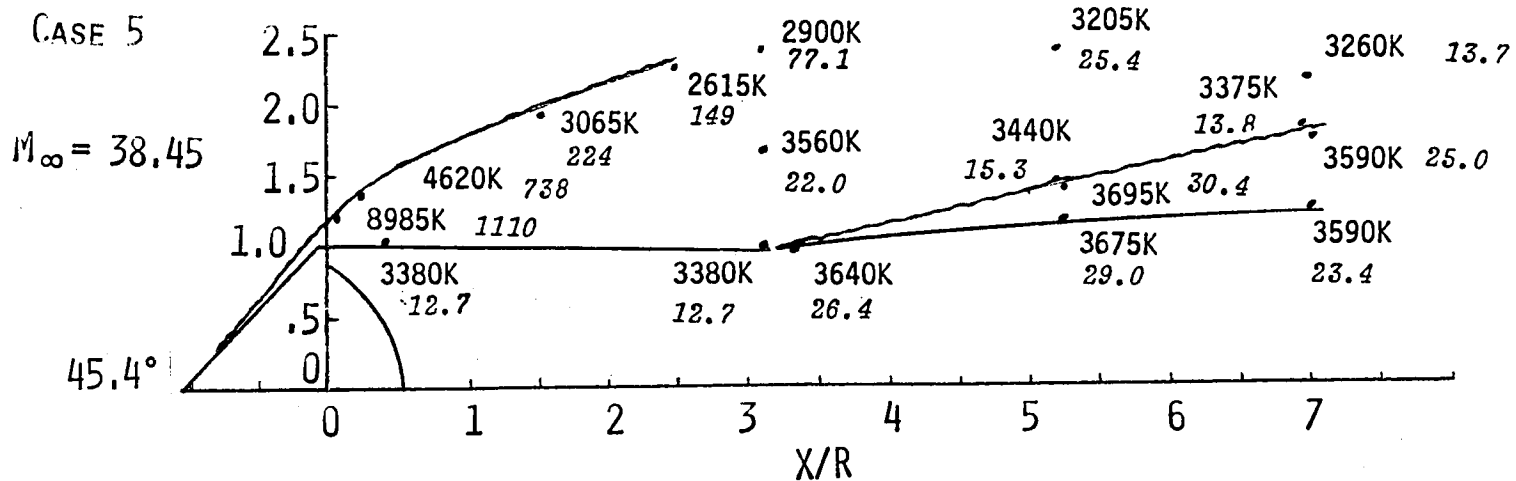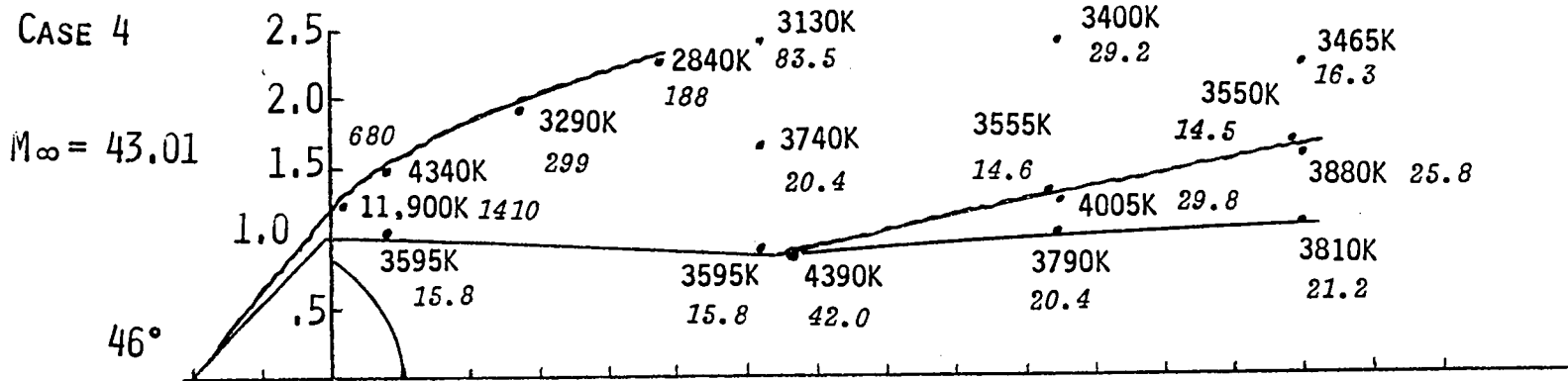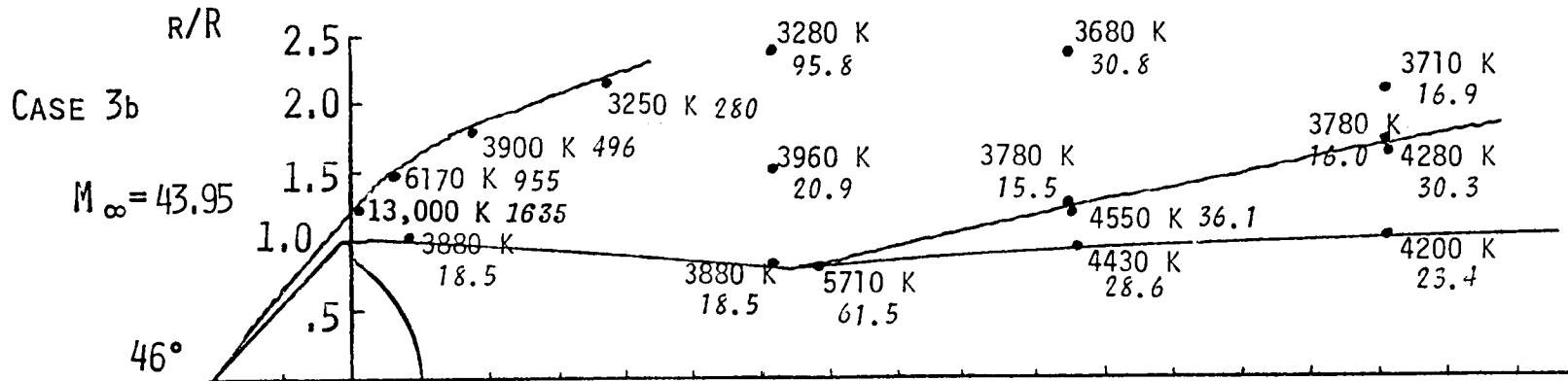
Fig. 15   Comparison of Inviscid Wakes
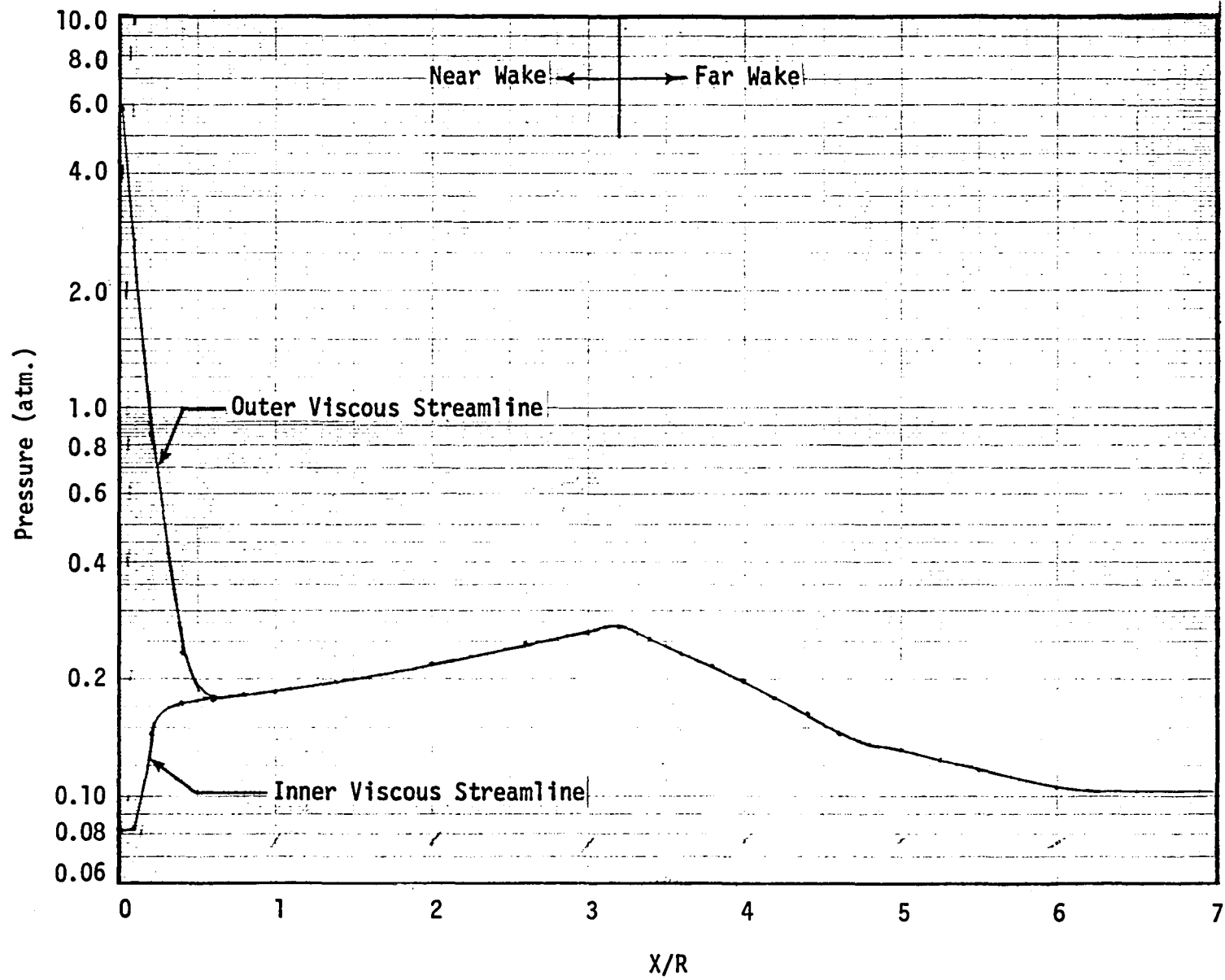
Fig. 16　Viscous Wake Streamline Pressures for Case 3b
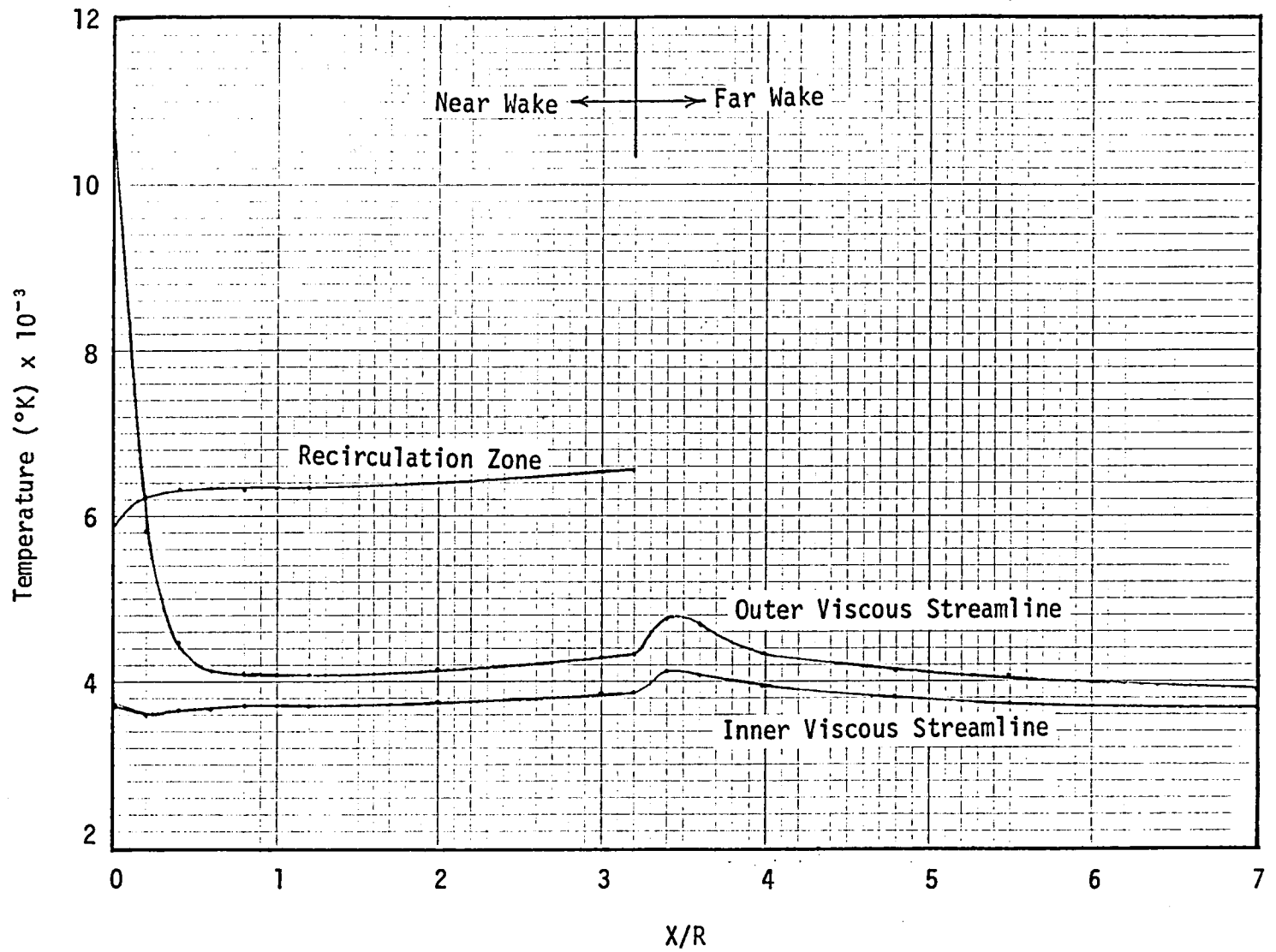
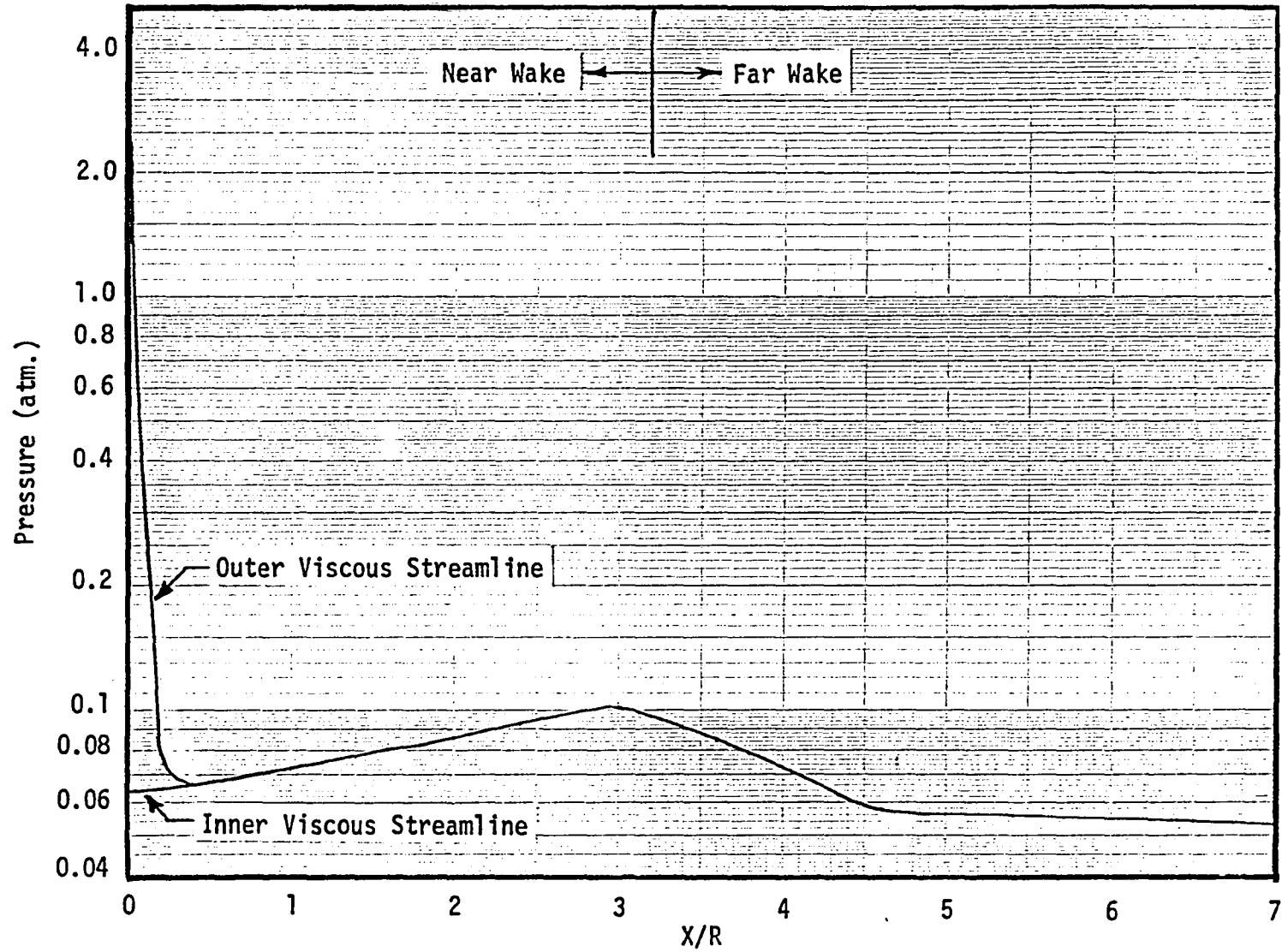Fig. 17   Viscous Wake Streamlines and Recirculation Zone Temperatures for Case 3b

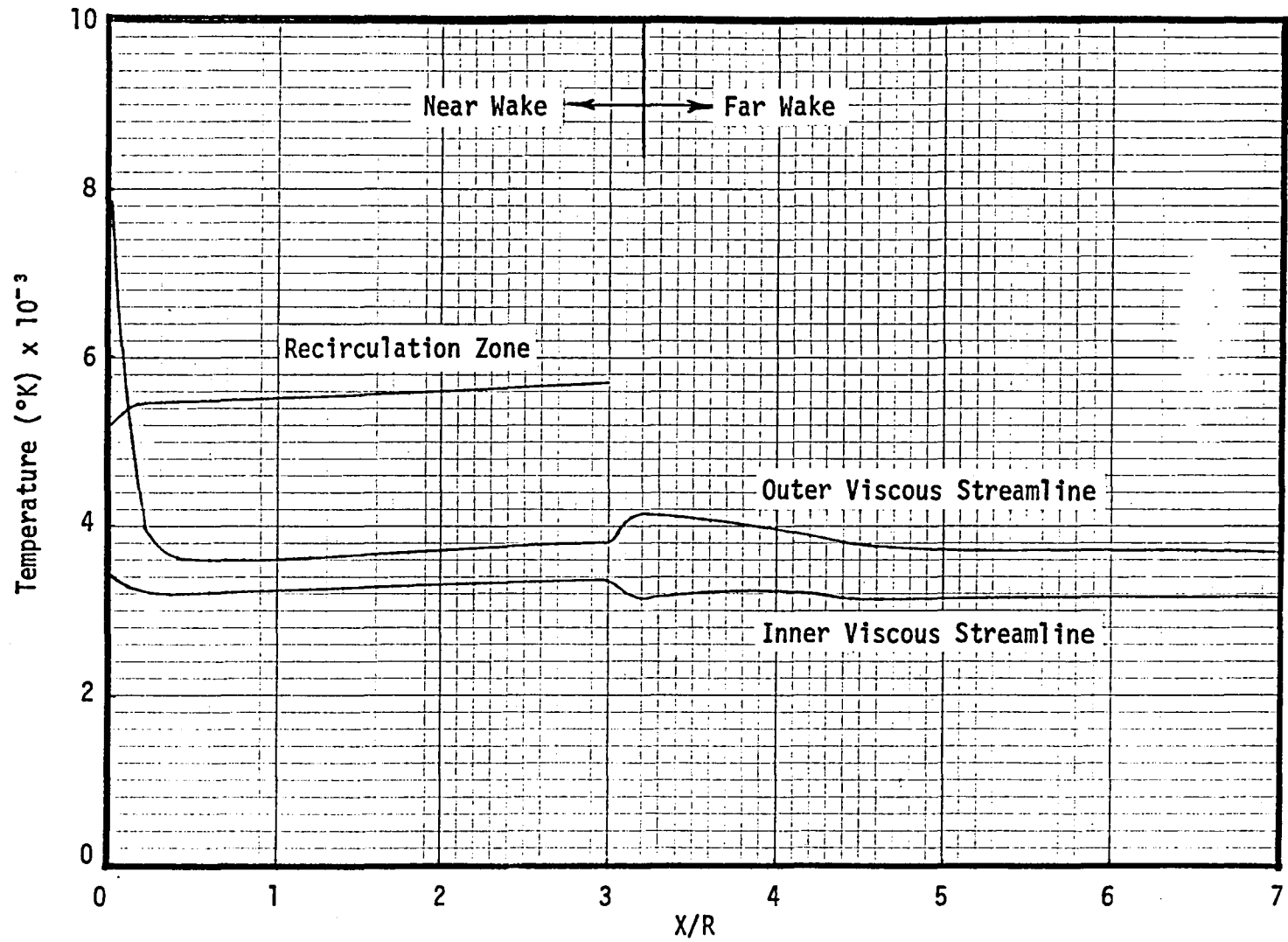Fig. 18 Viscous Wake Streamline Pressures for Case 4

47

Fig. 19 Viscous Wake Streamlines and Recirculation Zone Temperatures for Case 4
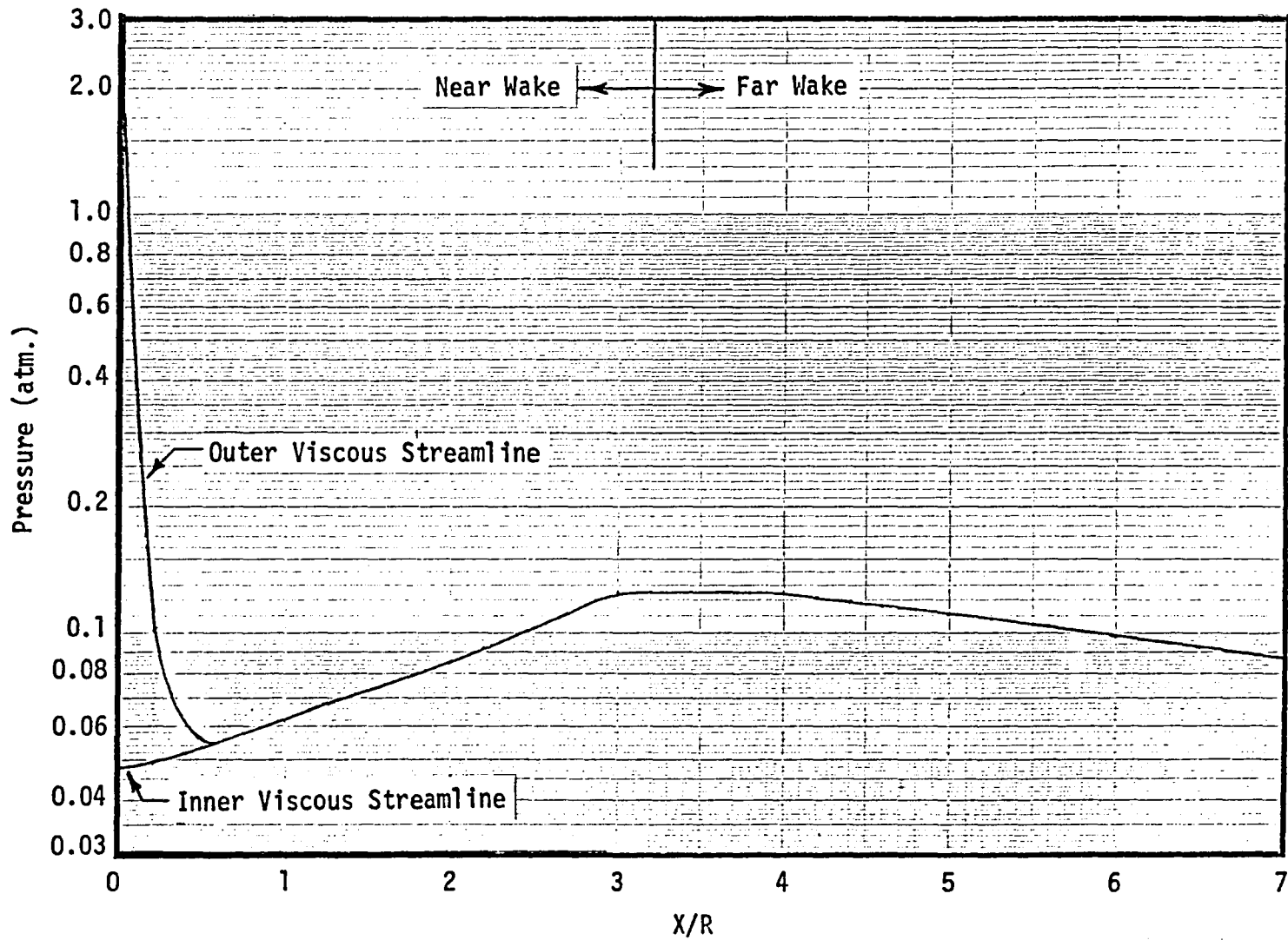
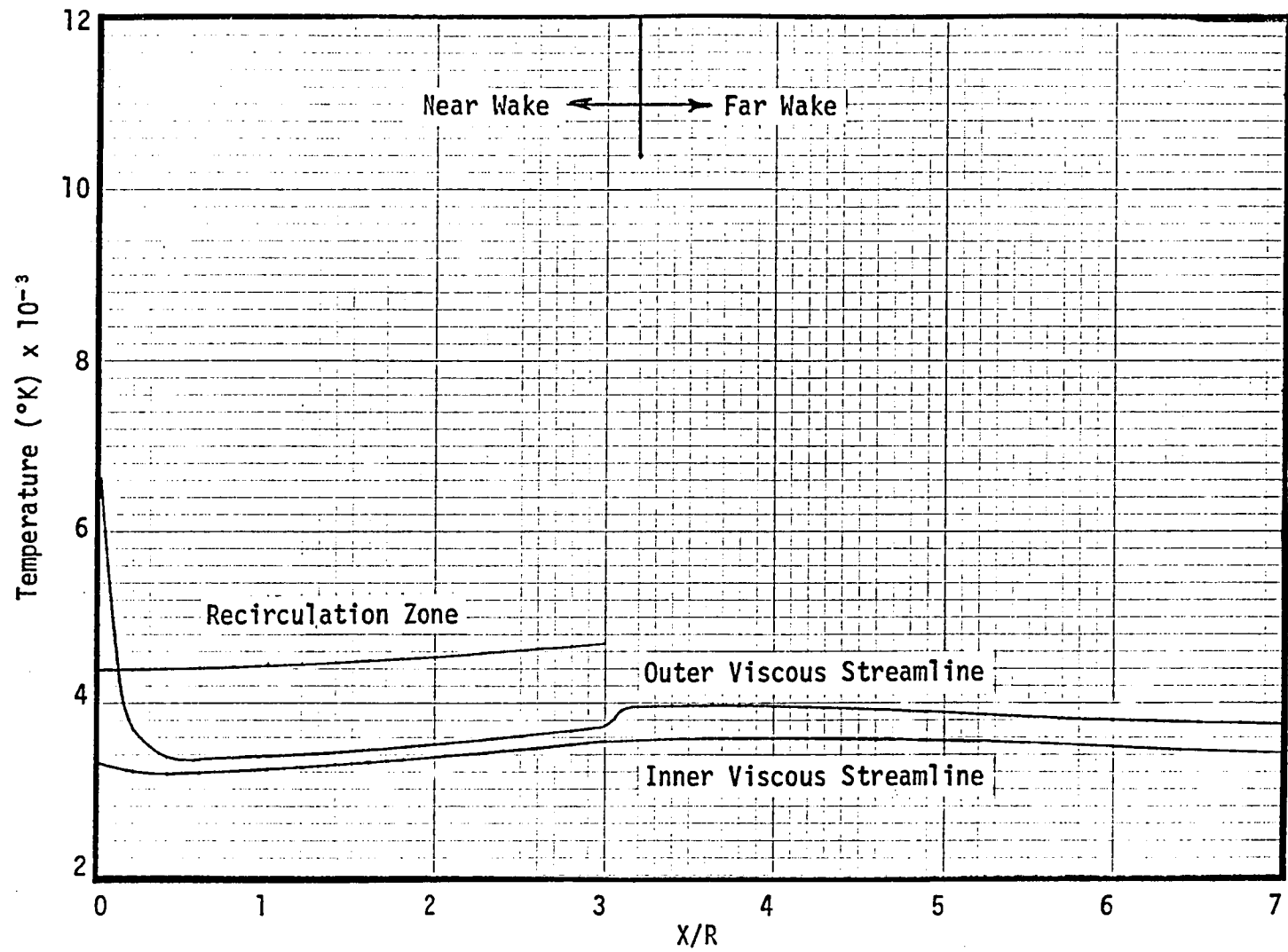Fig. 20 Viscous Wake Streamline Pressures for Case 5

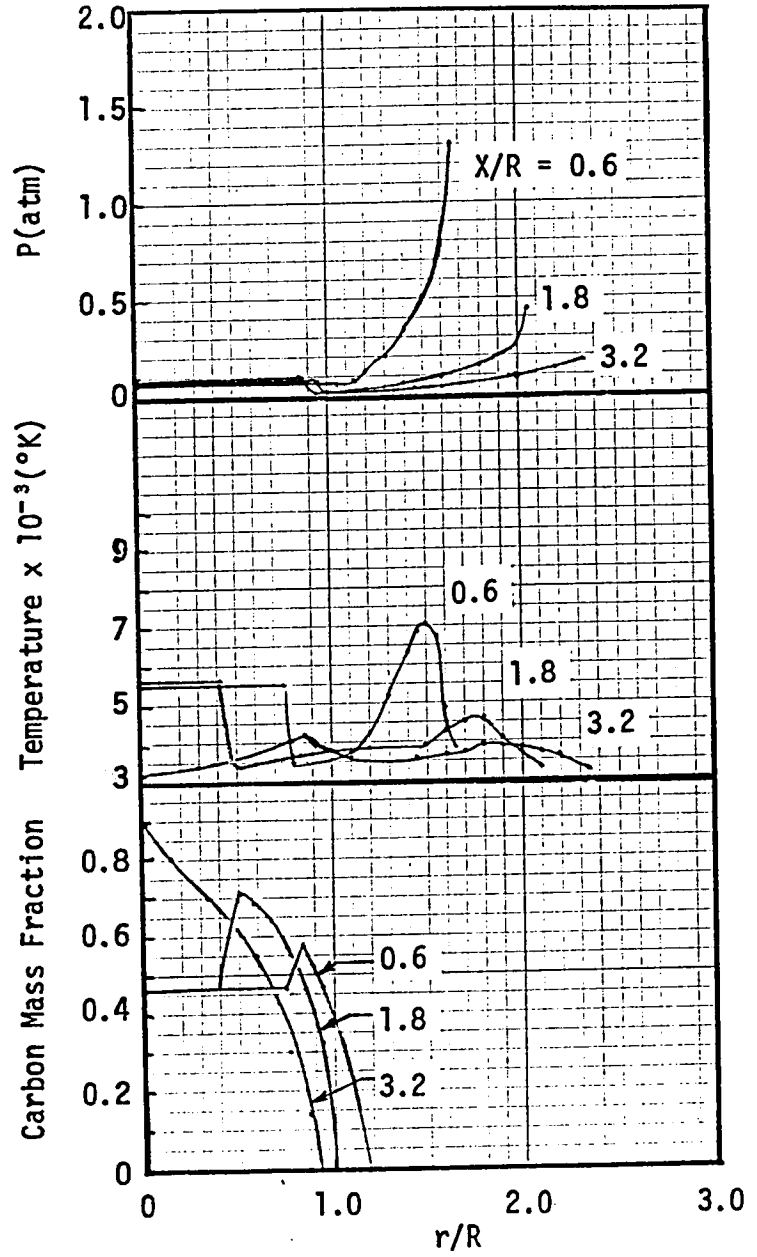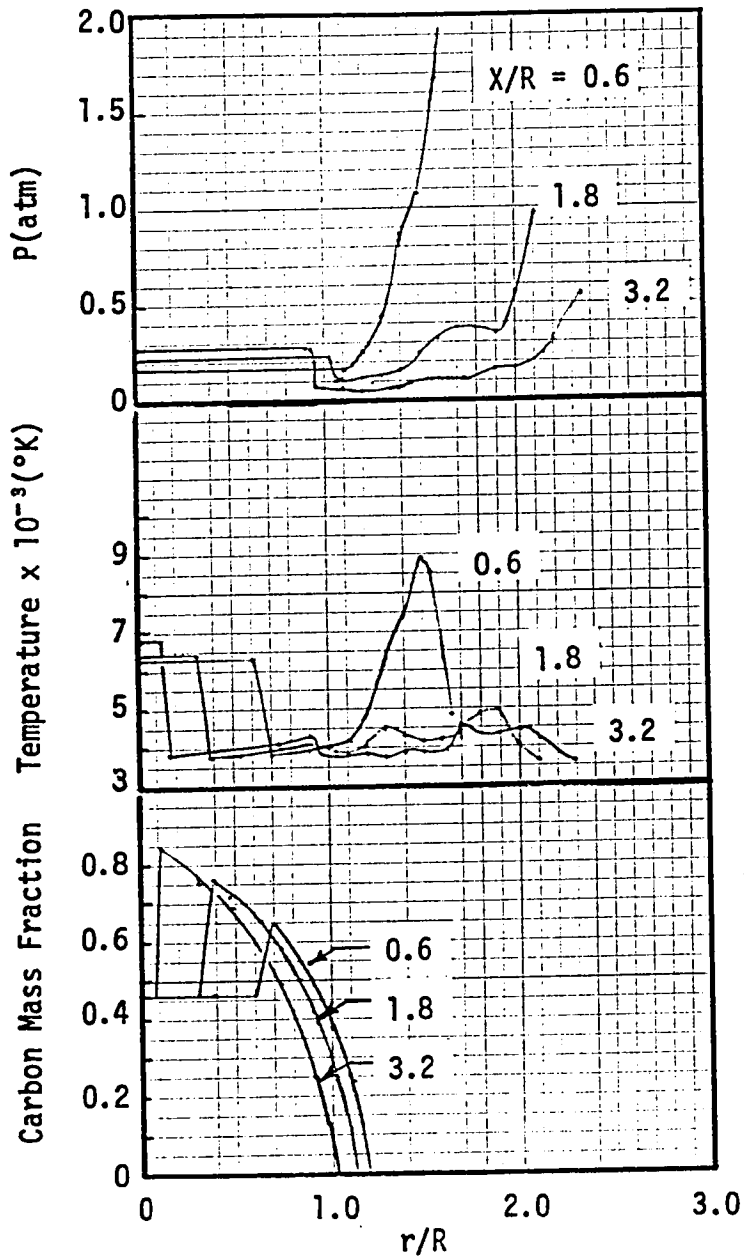Fig. 21 Viscous Wake Streamlines and Recirculation Zone Temperatures for Case 5
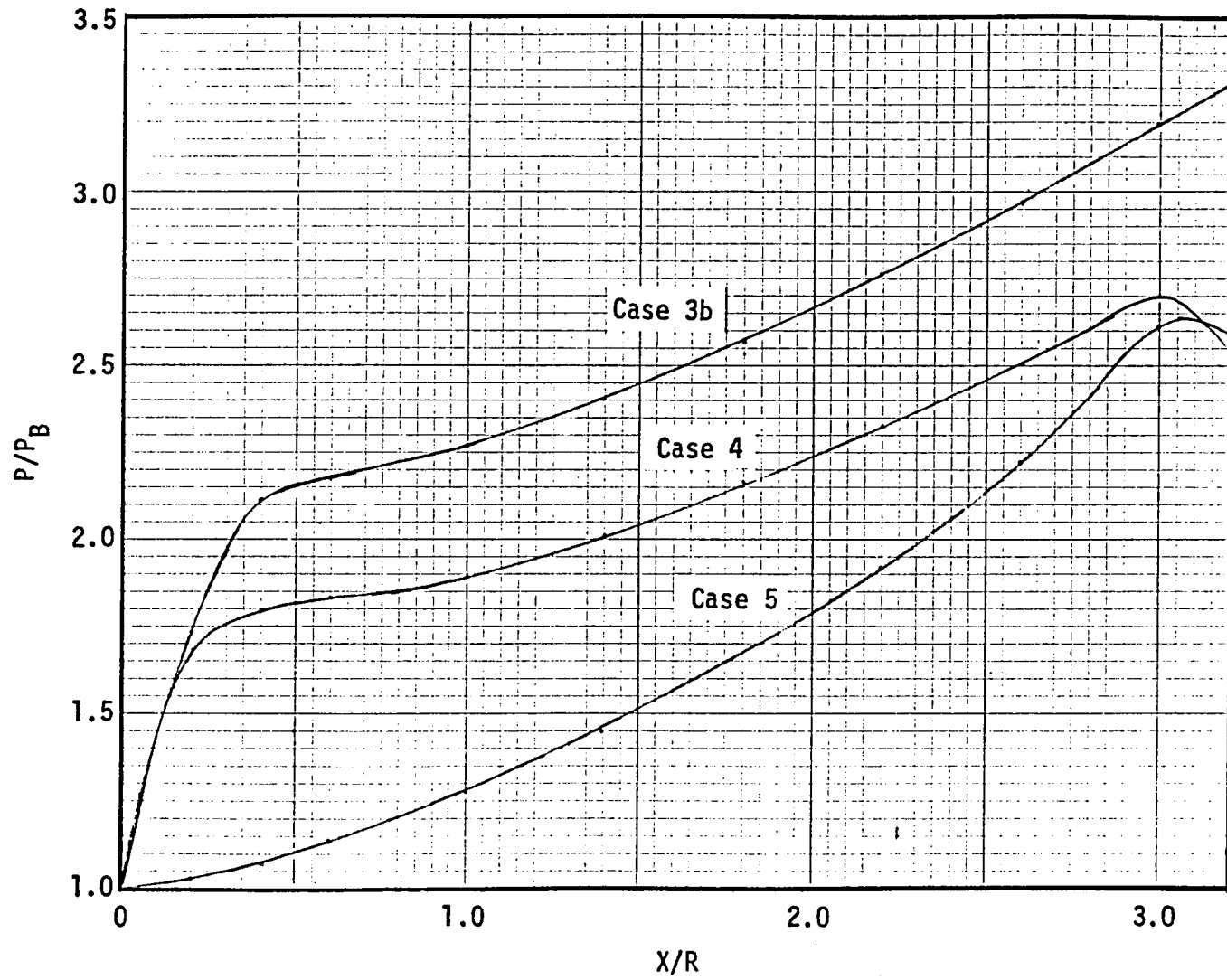
Fig. 22 Comparison of Near Wake Radial Profiles

Fig. 23 Near Wake Nondimensional Pressure Distributions

1. Report No. NASA CR-159235	2. Government Accession No.	3. Recipient's Catalog No.
4. Title and Subtitle WAKE FLOWFIELDS FOR JOVIAN PROBE		5. Report Date March 1980
		6. Performing Organization Code
7. Author(s) C. D. Engel and L. M. Hair		8. Performing Organization Report No.
		10. Work Unit No.
9. Performing Organization Name and Address REMTECH, Inc. 2603 Artie Street, Suite 21 Huntsville, AL 35805		11. Contract or Grant No. NAS1-15819
		13. Type of Report and Period Covered Contractor Report
12. Sponsoring Agency Name and Address National Aeronautics and Space Administration Langley Research Center Hampton, VA 23665		14. Sponsoring Agency Code

15. Supplementary Notes

Contract Monitor: James Moss, NASA, Langley Research Center

16. Abstract

A study was conducted to math model the wake flowfield developed by the Galileo probe as it enters the Jovian atmosphere. The wake produced by the probe is highly energetic, yielding both convective and radiative heat inputs to the base of the probe. A component math model for the inviscid near and far wake, the viscous near and far wake, and near wake recirculation zone was developed. Equilibrium thermodynamics were used for both the ablation and atmospheric species. Flowfields for three entry conditions were calculated. The near viscous wake was found to exhibit a variable axial pressure distribution with the neck pressure approximately three times the base pressure. Peak wake flowfield temperatures were found to be in proportion to forebody post shock temperatures.

17. Key Words (Suggested by Author(s)) Wake flowfields Galileo probe Hypersonic wakes Jupiter entry	18. Distribution Statement Unclassified - Unlimited
19. Security Classif. (of this report) Unclassified	20. Security Classif. (of this page) Unclassified	21. No. of Pages 52	22. Price*

N-305   For sale by the National Technical Information Service, Springfield, Virginia 22161